DOWNSCALED TROPICAL CYLCONES IN SIMULATIONS OF THE LAST GLACIAL MAXIMUM

An Undergraduate Research Scholars Thesis

by

QUINTON LAWTON

Submitted to the Undergraduate Research Scholars program at
Texas A&M University
in partial fulfillment of the requirements for the designation as an

UNDERGRADUATE RESEARCH SCHOLAR

Approved by Research Advisor: Dr. Robert Korty

May 2018

Major: Meteorology

TABLE OF CONTENTS

ABSTRACT

Downscaled Tropical Cyclones in Simulations of the Last Glacial Maximum

Quinton Lawton
Department of Atmospheric Sciences
Texas A&M University

Research Advisor: Dr. Robert Korty
Department of Atmospheric Sciences
Texas A&M University

A prominent area of current study is how tropical cyclone (TC) behavior will respond to future changes in global climate. One way to complement this research is by analyzing TC characteristics in simulations of past climates. In this project, we analyze the properties of TCs statistically downscaled from several climate simulations using the Coupled Hurricane Intensity Prediction System (CHIPS). This is done utilizing climate simulations of the Last Glacial Maximum (LGM) and 20th Century from three members of the Paleoclimate Modelling Intercomparision Project Phase III (PMIP3). We compare changes in large-scale tropical cyclone genesis factors to that of atmospheric circulations to better understand underlying sources of inter-model variability. Results from all three models depict a higher proportion of TCs reaching high (Category 4 and 5) intensities in the 20th Century climate compared to the colder LGM climate. Changes in TC annual frequency are more variable, with two models producing increased annual frequency with LGM to 20th Century warming and one model producing the opposite. This analysis provides insight on how tropical cyclones may have behaved during the LGM and can be compared to future projections of TC response to anthropogenic climate change.

DEDICATION

This thesis is dedicated to the memory of my good friend, Sean Weinstein. His character, kindness, integrity, and most of all, friendship, will never be forgotten.

ACKNOWLEDGEMENTS

I would like to thank my research advisor, Dr. Korty, for his guidance and support throughout the course of this research. Thanks also go to Ryan Zamora for his work processing data essential to this project, and to Dr. Kerry Emanuel at the Massachusetts Institute of Technology for supplying our group with the downscaled data. I would also like to thank the many faculty in the Department of Atmospheric Sciences for their work in ensuring undergraduates such as myself have abundant opportunities in high-impact experiences, such as research.

Finally, I would like to thank my friends and family for their unwavering support as I continue to pursue my dreams.

NOMENCLATURE

TC	Tropical Cyclone
PMIP3	Paleoclimate Modelling Intercomparision Project Phase III
YA	Years Ago
KYA	Thousand Years Ago
LGM	Last Glacial Maximum
20C	20^{th} Century

CHAPTER I

INTRODUCTION

Tropical Cyclones (TCs) can have devastating physical and socio-economic impacts on the modern world. A prominent area of current concern is how trends in TC intensity, tracks, longevity, and annual cycle will respond to changes in global climate. One way to better understand and contextualize projections of future changes in TCs is to study their behavior in past climates (Koh et. al., 2015). One of the primary motivations for this is rooted in the complex response of thermodynamic parameters to large-scale climate change.

Recent work has focused on understanding the potential impact of human activities on TC intensity and behavior (Sobel 2016). A relationship between an environment's potential intensity (PI)- essentially an upper-boundary on hurricane strength based on the atmospheric thermodynamic profile- and the average intensity of TCs has been established (Bryan and Rotunno 2009; Wang et. al. 2014; Sobel 2016). Research has also suggested that overall values of PI will increase with a warming climate, with regional variations (Yu et. al. 2010, Sobel 2016). This strongly suggests that a warming climate supports greater average TC intensity- an argument which has been corroborated by many simulations and observations (Emanuel 2005; Bender et. al. 2010, Knutson et. al. 2015, Sobel 2016). However, less certain are the impacts of warming on TC frequency, which has not yet been successfully explained by physical theory (Sobel 2016). Many direct simulations of TCs have shown a reduced annual frequency in TCs with warming climate (e.g. Murakami et. al. 2012; Knutson et. al. 2015; Sobel 2016). The statistical methodology used in this analysis, however, has shown the reverse (e.g. Emanuel 2015). Studying the response of TCs to climate change within paleoclimate simulations- as is

done in this analysis- can help evaluate how robust these established trends are for climate states much different than the modern day.

Changes in individual environmental conditions, such as SST and upper level temperatures, can have complicated effects on thermodynamic properties associated with TC formation and intensification. In a seminal paper, Gray (1968) identified several conditions deemed "necessary but not sufficient" for TC formation. Among these were sea-surface temperatures (SST) of 26°C or above, enhanced values of 700mb relative humidity, and a vertical temperature profile supporting conditional instability. Furthermore, Emanuel (1986) argued that the fundamental physics controlling TCs was an air-sea enthalpy exchange resulting from the thermodynamic disequilibrium between the sea surface and lower atmosphere. Many parameters have been developed to describe the impact these conditions have on TCs. These include previously mentioned potential intensity (PI), as well as the Genesis Potential Index (GPI)- an empirical index that relates large-scale conditions to TC genesis. Variations in these parameters- indicative of the overall environment- are often highly regionalized. An example of this is depicted in Korty et. al. (2012), where a simulated decrease in global temperature during the Last Glacial Maximum (LGM) did not result in a uniform drop in parameters such as PI or the GPI. Rather, PI and GPI in LGM simulations remained similar to the pre-industrial control in many parts of the world, with regional pockets of increases and decreases (Korty et. al. 2012). An analysis by Koh and Brierley (2015) on Paleoclimate Modelling Intercomparision Project Phase III (PMIP3) simulations of the LGM showed a similar overall global consistency in PI and GPI between the LGM and pre-industrial control, with regional increases in the North Pacific basin and decreases in the North Atlantic basin.

While spatial and temporal depictions of environmental properties provide important insight on TC formation and development potential, in many cases they only provide indirect evidence of these characteristics. Looking at long-term averages also neglects much of the inherent variability of local environmental conditions on short and medium time-scales. We suspect that directly downscaling TCs from these climate simulations will provide a more robust representation of TC response, while still being comparable to depictions of thermodynamic controls. In this paper, we expand on previous work by analyzing the behavior of TCs directly downscaled from three simulations of the Last Glacial Maximum (around 21 KYA). Of great interest to us were the underlying shifts in global circulation patterns that lead to inter-model variability in downscaled TCs and related environmental factors; the reasons for these are examined in the following section.

Motivations

There are many motivations for studying TCs in simulations of the LGM. For one, important differences are known to exist in climate characteristics between the LGM and the 20th Century. Major changes in climate between these two time-periods allow environmental controls on important aspects of TC behavior to be easily discernible. Important shifts in atmospheric and oceanic circulations are also suspected to have taken place during the LGM, allowing underlying sources for inter-model variability to be more readily identified. An additional motivation was that climate characteristics in these time periods have been more reliably reconstructed (through geological proxies) than some other periods of significant climate change in the geological past. This results in more confidence that these climate simulations can be reasonably calibrated to evidence from the geologic record. In contrast, projections of future climate change have no

analogous calibration technique. A discussion of environmental characteristics, patterns, and external forcing can be found in a later section.

Previous studies employing our chosen statistical downscaling method have shown significant variability in annual cycle and spatial patterns of TCs between model simulations of the same climate state (e.g. Fedorov et. al. 2010, Emanuel et. al. 2008, Emanuel 2013, Korty et al. 2017). This can be largely attributed to differences in model response to the identical external climate forcing, resulting in differing depictions of global circulation patterns. These shifts can greatly alter the spatial distribution and magnitude of environmental factors important to TC genesis and intensification. Thus, in interpreting various model depictions of TC trends, it is immensely important to understand underlying shifts in global atmospheric and oceanic circulations. Doing so allows a better understanding of individual model biases and response to be developed. While this paper focuses on simulations of paleoclimate states, comparing the variability between downscaled TCs in future climate projections will also be important to better quantify the predicted response of TCs to anthropogenic climate change. Through an understanding of intermodel variability, downscaled TC trends, and related environmental factors, an overall picture of TC activity in the LGM can be produced.

There also is evidence suggesting the possibility of partial reconstruction- through geological proxies- of the historic TC record. Liu and Fearn (1993) demonstrated that a record of significant hurricane landfalls during the Late Holocene could be obtained through the analysis of coastal lake sediments (see also Donnelly et. al. 2001). Reconstructions up to 12,000 years ago have also been shown possible using deep-sea sediment cores (Toomey et. al. 2013, Denommee et. al. 2014, Toomey et. al. 2017). Current reconstruction techniques have many limitations- there is a scarcity of suitable cores, data is only available at the sample site, and only

limited information on TC characteristics can be deduced. Nevertheless, advancements in this area could allow future comparisons of TC reconstructions to downscaled simulations during the Last Glacial Maximum. This again provides an advantage to modelling TC behavior during these time periods, as a historical record does not exist for future projections.

Background on Tropical Cyclone Downscaling

One way to study the response of TCs to climate change is to directly simulate them in a variety of climate states. This allows researchers to directly compare the statistical distributions of TC characteristics and their associated environmental conditions. Furthermore, TC simulations allow both predictions for the future and depictions of the past (such as the LGM) to be made.

Despite their usefulness, climate simulations are often subject to large amounts of inter-model variability due to computational and theoretical limitations. Even more, most climate simulations have spatial and temporal resolutions too coarse to reliably resolve TCs in their output. As a result, many previous studies on TCs in paleoclimates and future projections have focused on the trends of environmental parameters known to be important for TC formation and intensification. Attempts have been made to develop a robust genesis potential index from these environmental parameters that remain valid across a variety of climate states (Korty et. al. 2012). One such index- GPI- was developed in Emanuel and Nolan (2004) and subsequently modified by Emanuel et. al. (2008) and Korty et. al. (2012). While useful for analysis, these indices are largely empirical.

A statistical downscaling method used to study TCs behavior in climate simulations was developed by Emanuel (2006). In this method, a set number TC are synthetically downscaled from climate simulations. The behavior of these TCs is simulated using the Coupled Hurricane

Intensity System (CHIPS). To do so, CHIPS ingests information on a TCs residual environment from a climate simulation as boundary conditions. This process allows TC characteristics such as intensity and movement to be studied within coarse climate models otherwise unsuitable for this research (Emanuel 2006 and Emanuel et. al. 2008). Previous work using this method showed success in recreating the annual cycle and variability in TCs during the 20th century (Emanuel et al. 2008). As with many methods of TC downscaling, however, this method is subject to the large inter-model variability present in climate models. We utilized this method for our analysis, as we felt it offered the most flexibility and reliability for looking at PMIP3 model output. A more thorough description of this methodology, as well as specific data inputs and outputs, is provided in Chapter II.

Characteristics of Select Climate States

To understand and quantify general environmental conditions in the LGM and present-day climates, a combination of geological proxies, computer modelling, and observational data has been used. While a complete description of the techniques and results from these analyzes is outside the scope of this paper, we have summarized the relevant background on what is currently known about these climates. PMIP3 climate experiments were conducted under CMIP5 protocols (Taylor et. al. 2009; Taylor et. al. 2012).

Last Glacial Maximum

The Last Glacial Maximum (LGM) occurred approximately 21,000 years ago. Forcing for LGM climate was a result of large changes in ice sheet coverage, greenhouse gases, sea level, and vegetation patterns (Otto-Bliesner et al 2005). Changes in insolation at the top of the atmosphere- while slightly different than during the 20th century- likely only played a secondary role. During the LGM, ice covered a large portion of the land and sea area at higher latitudes,

and surface temperatures were much colder globally (Broccoli 2000). Research has suggested that surface temperatures over the tropics were around 2°C colder during the LGM compared to 20th Century climate and more than 30°C colder in high latitudes, where permanent ice sheets covered large portions of the continent (Broccoli 2000). Atmospheric concentrations of CO_2 have been estimated at around 185 ppm, much lower than during the 20th Century (Braconnot et. al. 2007, Brady et. al. 2013).

20th Century

In our analysis the 20th Century is defined as the years 1980 through 2005. All PMIP3 simulations have been set with identical climate forcing as defined by model standards for the last millennium, detailed by Schmidt et. al. 2011. Ice sheets, topography and coastlines are all at their modern-day extent. Variations of Earth's orbital precession are accounted for, with Earth making its closest approach to the Sun at the beginning of the Northern Hemisphere winter (Schmidt et. al. 2011). Trace gases- including CO_2, CH_4, N_2O- are all set based on yearly reconstructions.

CHAPTER II

METHODS

In this analysis, tropical cyclones are downscaled using climate data from three members of the Paleoclimate Modelling Intercomparision Project Phase III- CCSM4, MRI5, and MPI5. MRI5 and MPI5 are henceforth referred to MRI and MPI, respectively. Two climate states are analyzed- the Last Glacial Maximum and the 20th Century. We analyze storms generated using the methodology established by Emanuel (2006) and used in later analyses of tropical cyclones in future and past climates (e.g. Emanuel et. al. 2008, Emanuel 2013, and Korty et. al. 2017). We are primarily interested in differences in tropical cyclone characteristics between climate states.

Downscaling TCs from PMIP3 Simulations using CHIPS

In this method, broad axisymmetric vortices of sub-tropical cyclone intensity- henceforth known as TC "seeds"- are randomly distributed across the globe. Each TC seed starts as a weak disturbance, with maximum wind speeds of 25 knots or less. Data was only stored for TC seeds that reach tropical storm intensity (~34kt) at some point in their lives. TC seeds that do not reach this intensity are discarded and not included in the final analysis. This allowed us to generate an equal and large number of tropical cyclones for each climate state and compare the number of seeds required in each case to do so. Table 1 shows the total number of tropical cyclones that were generated for each simulation and climate state.

Table 1

Total Number of Downscaled Tropical Cyclones for Each Simulation and Climate State			
	CCSM4	**MRI5**	**MPI5**
20th Century	5200	5200	5200
Last Glacial Maximum	6000	6000	6000

A simulation of each seed is initialized using the Coupled Hurricane Intensity Prediction System (CHIPS), which parses the storm through conditions ingested from the global model (Emanuel et. al. 2004). In our analysis, the CHIPS model incorporates PMIP3 climate data at and around the location of each TC seed as boundary conditions. To better represent the typical variability of atmospheric conditions in relation to climatology, incorporated wind data is not of the monthly average itself but of random pull from a distribution centered at the monthly average with variance determined from 6-hourly data. Other environmental properties- including sea-surface temperature- are assumed to have minimal variability and their monthly averages are directly incorporated. Utilized climate data span 30 years for the LGM climate and 25 years for the 20th Century climate. Storm motion is determined using a simple beta and wind advection model. This calculates TC advection from the 250mb and 850mb level winds and corrects it for beta-drift.

It should be noted that the vast majority of TC seeds fail to strengthen to tropical storm intensity. This is in large part due to the randomness of TC seed placement, as seeds have a high probability of being placed in regions or at a time of year inhospitable to tropical cyclone development. While information about TC seeds that do not achieve genesis is not stored, the

total number of seeds needed to generate the final number of TCs is. This is later used to calculate the global annual frequency of each climate state and simulation.

PMIP3 simulations are all run with the same external forcing for each climate state being simulated. These correspond to specific forcing discussed in the introduction, such as CO_2, CH_4, and ice sheet position. A more detailed discussion of how these forcing parameters were selected can be found in work done by Braconnot et. al. (2012). Of primary interest to us was how each model independently resolved features that are significant to TC development and intensification despite identical forcing. Many of the thermodynamic parameters important to these processes are highly regionally and locally sensitive, which could theoretically lead to large variations in TC activity.

Measuring Environmental Factors

Environmental Parameters

Holland (1997) describes a theoretical maximum potential sustained wind velocity for a theoretical TC that is based on an environment's thermodynamic properties. This so-called maximum potential intensity (MPI) gives an estimate of the lowest possible TC pressure for a given environment. This method has seen widespread operational and research use but is not as useful for the kind of analysis we were pursuing. Instead, we used a method approximating the maximum sustained wind speed possible for a TC in a given environment. This can be done using the conceptual model argued by Emanuel (1986), equating a TC as a near perfect representation of a Carnot Heat Engine. By equating an approximation of the dissipated kinetic energy due to friction at the surface to the highest possible work that could be done by a TC in an environment (based on its thermodynamic profile), maximum sustained wind speed can be calculated (Emanuel 1995; Emanuel 2003). This upper-bound on wind speed is referred to as

potential intensity (PI) and is a convenient way to spatially represent the thermodynamic favorability of a region. Equation 1 depicts a thermodynamically-derived calculation of PI. While useful, PI does not give a complete picture of an environment's favorability for TC intensification. This is because thermodynamic favorability can be heavily modulated by wind shear, which is detrimental to TCs in large quantities, along with other external properties such as dust and aerosols.

$$V_{max} = \sqrt{\frac{Ck}{Cd} * \frac{T_s - T_O}{T_O} * (K_0^* - K)}$$

Equation 1

While Equation 1 is useful for understanding the environmental factors influencing PI, it is not the most computationally effective method. We instead used a method developed by Bister and Emanuel (2002), which utilizes a simulation's atmospheric profile to calculate convective available potential energy (CAPE) and the resulting PI.

Vertical wind shear in this analysis was defined as the difference in wind speed and direction between the 250-mb height level and the 850-mb height level. Vertical wind shear has a detrimental effect on tropical cyclone formation and intensification (Gray 1968). This is thought to result from wind shear's role in mixing lower entropy air into the TC eyewall while disturbing typical mid-level entropy flux (Gu et. al. 2015). Storms in these high wind shear environments require additional energy to saturate the same column of air, depleting the efficiency of a TCs thermodynamic conversion of energy to work. It also can effectively "tilt' a TCs vortex. As a result, vertical wind shear is an important factor for determining the environmental favorability of simulated climate states.

Combined Metrics- PDI and CGI

Because thermodynamic favorability and vertical wind shear both have direct effects on TC development and intensification, incorporating these factors into a single metric is advantageous for cross-simulation comparison. One such metric, named the Cyclone Genesis Index (CGI), was developed by Bruyere et. al. (2012). CGI combines the effects of potential intensity and vertical wind shear into one parameter. Equation 2 shows the exact formula for CGI used in this analysis.

$$\boldsymbol{CGI = \left(\frac{PI}{70}\right)^{3} * [1 + 0.1(V_{shear})]^{-2}}$$

Equation 2

It should be noted that CGI is only one weighted metric of environmental favorability. In future work, other weighted metrics of environmental factors- such as ventilation- will be used as a comparison to CGI (Tang and Emanuel 2010).

To better characterize changes in TC characteristics, it is useful to define a parameter collectively quantifying TC track density, intensity, and frequency over a given area. Emanuel (2005) defines the Power Dissipation Index (PDI)- itself an approximation of Power Dissipation- as Equation 1 below, where τ is a TC's duration and V_{max} is its maximum sustained wind.

$$\boldsymbol{PDI = \int_{0}^{\tau} (V^{3}_{max})\, dt}$$

Equation 3

PDI is similar in concept to the Accumulated Cyclone Energy (ACE), with PDI using a cube of the maximum wind speed while ACE uses a square of the maximum wind speed. PDI's use of the cube of maximum wind speed relates to previous work showing that monetary loss due to TCs roughly rises with the cub of maximum wind speed (Southern et. al. 1979, Emanuel 2005). We use PDI as a combined indication of TC duration, track, and duration at a given point.

Similar to Korty et. al. (2017), we use an annual sum of downscaled TC PDI over an 5x5 latitude grid box. This is normalized by dividing by the km^2 grid box area.

Statistical Methods

In our analysis, both a spatial (grid point by grid point) and a basin-wide viewpoint are adopted. Additionally, all environmental parameters are averaged over the four most active months of TC activity- known as the "storm-season". To make inferences on suspected differences between each climate state's environment, we first tested for statistical significance.

The primary significance test utilized in this analysis was an unpaired, two-sample approximate T-test as shown in Equation 4. The utilized sample contained storm-season values for each year of a simulated climate state, taken either for a given grid-point or across an entire basin. $\bar{X}$ is the mean of this data, *s* is the standard deviation, and *n* is the number of data samples for each climate state. The null hypothesis is that of equal means ($\bar{X}_{20C} = \bar{X}_{LGM}$), and we evaluated significance at a 95% confidence level. Standard deviation was assumed equal for each climate state.

$$t = \frac{\bar{X}_{20C} - \bar{X}_{LGM}}{\sqrt{s^2(\frac{1}{n_{20C}} + \frac{1}{n_{LGM}})}}$$

Equation 4

Basin Regions and Masking

One primary and one secondary TC formation region were identified in each basin. Table 2 describes the boundaries for each of these selected regions. These areas were selected based on modern TC observations and the behavior of downscaled TCs in the simulations. Detailed statistics on environmental and downscaled TCs were generated for each region.

Table 2

Extent of Defined Boundaries for Analyzed Basins		
Basin	**Region Type**	**Boundaries**
Northern Atlantic	Primary	Gulf of Mexico, Caribbean Sea, Atlantic 10°N-20°N
	Secondary	Atlantic from North American coast to 60°W and 20°N-35°N
Western North Pacific	Primary	105°E to 150°E 5°N to 30°N
	Secondary	150°E to 180°E 5°N to 30°N

In addition to selective region-masking for some figures, all environmental outputs were masked by land. Because LGM climate has significantly lower sea level than 20th Century climate, LGM simulations had a larger overall land area and significant encroachment of land into shallow seas and gulfs. This could result in errors in thermodynamic calculations over regions considered to be ocean in 20th Century simulations but that encompass land in LGM simulations. As a result, figures were masked based on the land fraction specified for the simulation's LGM climate state. This limits statistical analysis to regions containing primarily ocean in both climate states, reducing error.

CHAPTER III

RESULTS

Global Characteristics of Downscaled TCs

One simple measurement of global TC activity is the annual frequency of occurrence across the globe. Our method of downscaling- in which a fixed number of TCs are generated for each climate state- necessitated that we utilize an indirect method of calculating annual frequency. To do so, we used the number of TC "seeds" as a way to measure overall annual frequency. Specifically, the ratio $\frac{\textbf{number of seeds used}}{\textbf{number of TCs generated}}$ was calculated for each model and climate state. This was calibrated to 80 TCs per year globally for the 20th Century climate state, in agreement with observations (Anthes 1982). From this, deviations in annual frequency were then calculated for the LGM simulations. If more seeds per downscaled TC were required for an LGM simulation compared to its 20th Century counterpart, its annual frequency would be calculated as some number below 80 TCs per year, and vice versa.

A drawback to this method is that it specifically normalizes each simulation's 20th Century to an annual frequency of 80 TCs per year. This number is not necessarily representative of the actual TC frequency that can be supported. It is unlikely that each simulation produced an identically favorable 20th Century climate- thus, normalizing this climate state to the same value removes the ability to directly compare annual frequencies across models. As a result, calculated annual frequencies are primarily used to compare the qualitative response to changing climate for a particular model.

Figure 1 depicts a comparison of the calculated annual frequency of TCs downscaled from LGM and 20th Century climate simulations. The MPI model and CCSM4 simulations both

show decreased global annual frequency for downscaled TCs during the LGM. Interestingly, the MRI model depicts an increase in global annual frequency during the LGM compared to its 20th Century. These LGM climate simulations are forced with significantly larger ice sheet extent and result in significantly cooler surface temperatures, both globally and in the tropics (Broccoli 2000). Thus, the MRI simulations indicates decreased TC frequency with warming, and the other two simulations indicate increased TC frequency with warming.

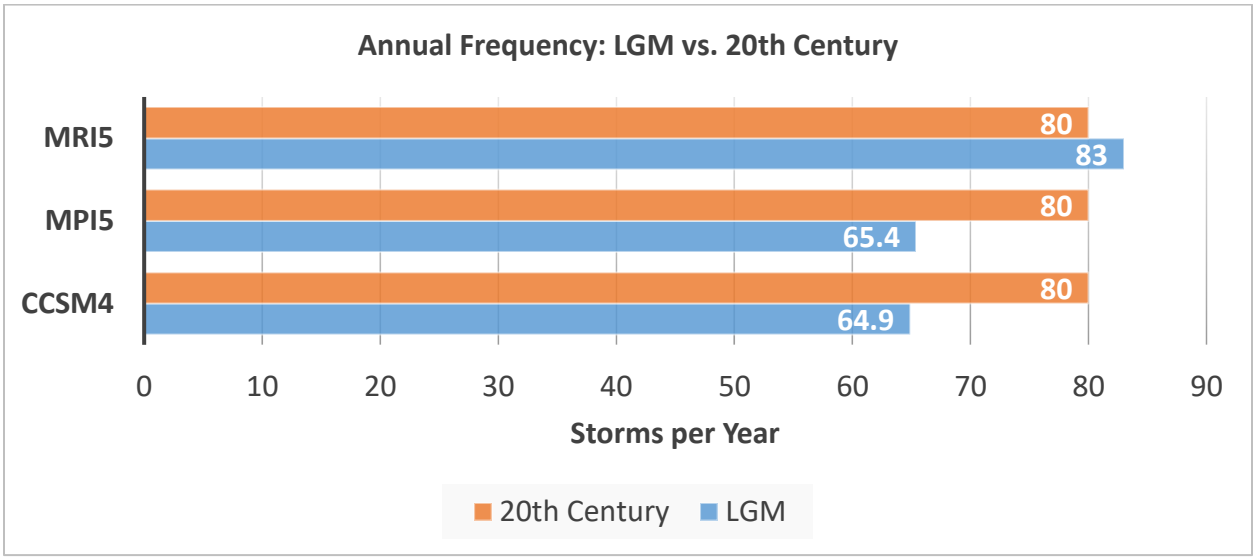

Figure 1- Graph comparing calculated TC annual frequency for each simulation and climate state. 20th Century climate states are in orange, while LGM climate states are in blue. Data was normalized to 80 storms per year for each simulation's 20th Century. Annual frequency is indirectly calculated from the ratio of needed TC seeds to the number of TCs generated.

In Figure 2, global distributions of maximum downscaled TC intensity are compared across climate states for all three models. To generate these histograms, TC counts for each climate state were normalized to a total TC count of 5200 storms. Intensity categorization was done using the Saffir-Simpson Hurricane Wind Scale, originally developed by Saffir (1973) and Simpson (1974). In all models, the majority of downscaled TCs only reach tropical storm or Category 1 strength, corresponding to maximum wind speeds between 34 and 82 knots. However, all three models showed a decrease in the proportional of downscaled storms reaching

Category 4 and 5 strengths in the LGM climate state as compared to the 20th Century. This indicates an increasing proportion of TCs reaching high intensities (Category 4-5) with global warming, in general agreement with results obtained from future climate projections (e.g. Sobel 2016). Both distributions of downscaled TC maximum intensity for MRI deviated from that of CCSM4 and MPI, with a broader distribution of TCs across all intensity categories.

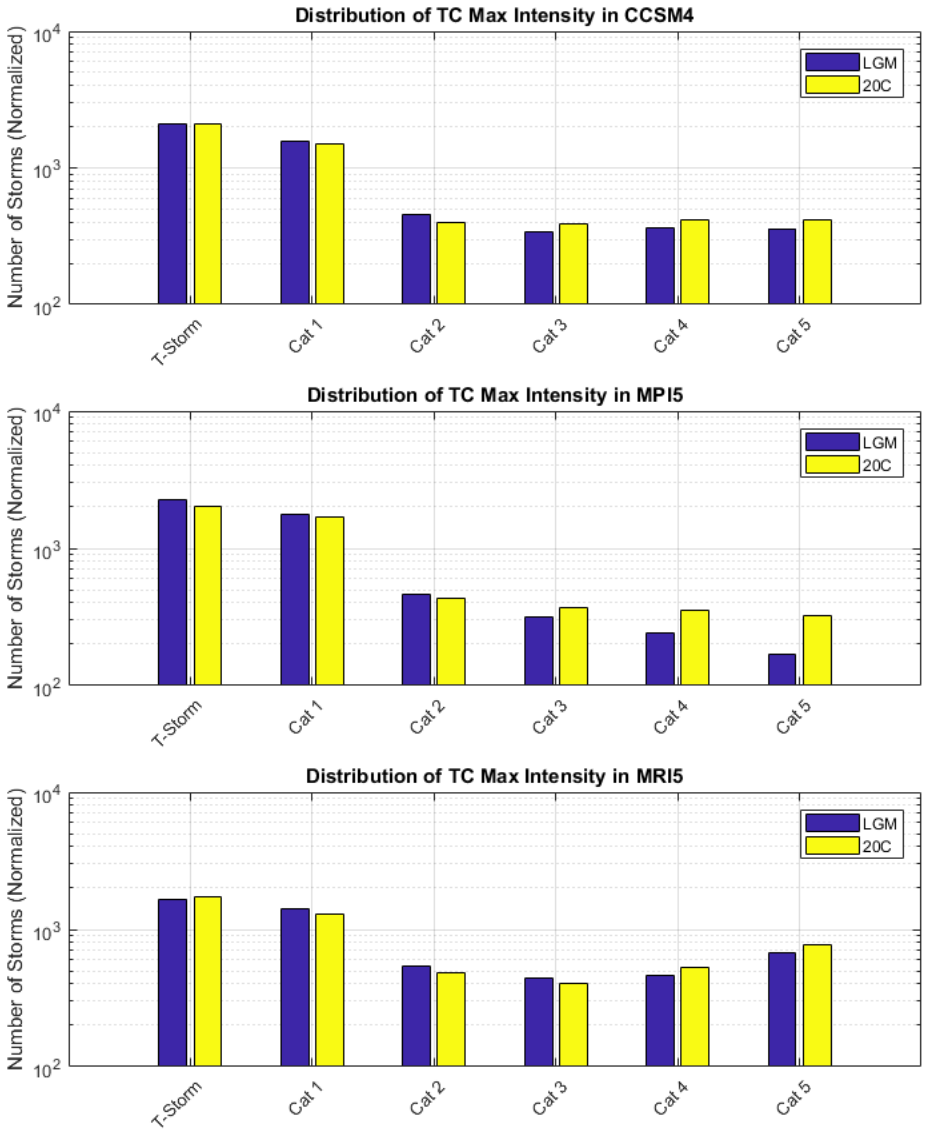

Figure 2- Comparison of the maximum intensity of downscaled TCs in LGM and 20th Century simulations. Three models are compared. Yellow bars indicate the 20th Century, and blue bars represent the LGM. Total TC counts have been normalized to that of the 20th Century, or 5200 storms. Maximum intensity is categorized using the Saffir-Simpson Hurricane Wind Scale.

Several parameters were used to analyze the characteristics of downscaled TCs and their residual environment. We primarily focused on spatial distributions within specific ocean basins. Most parameters were averaged over the range of four months corresponding to the highest amount of tropical cyclone activity for that region. This period of time- the "storm season"- was determined by the annual cycle of TCs for each simulation and climate state. A summary of the global annual cycle of downscaled TCs for the LGM and 20th Century, separated by hemisphere, is shown in Figure 3. A peak in TC activity during the early months of the year occurs in Southern Hemisphere, while a peak in activity during later months occurs in the Northern Hemisphere. For the most part, the temporal peak in TC activity for each simulation and climate state was similar for each climate state. Out-of-season storms did occur within each hemisphere, but their impact appears limited.

As shown in Figure 3, the top four months of activity are typically July through October for the Northern Hemisphere, and January through April for the Southern Hemisphere, with a few exceptions within shoulder-season month. In determining the storm-season, these exceptions were largely omitted in favor of a consistent period across all simulations. Doing so assumes that the effects of neglecting shoulder-season months were limited. Slight alteration of results due to this assumption is possible.

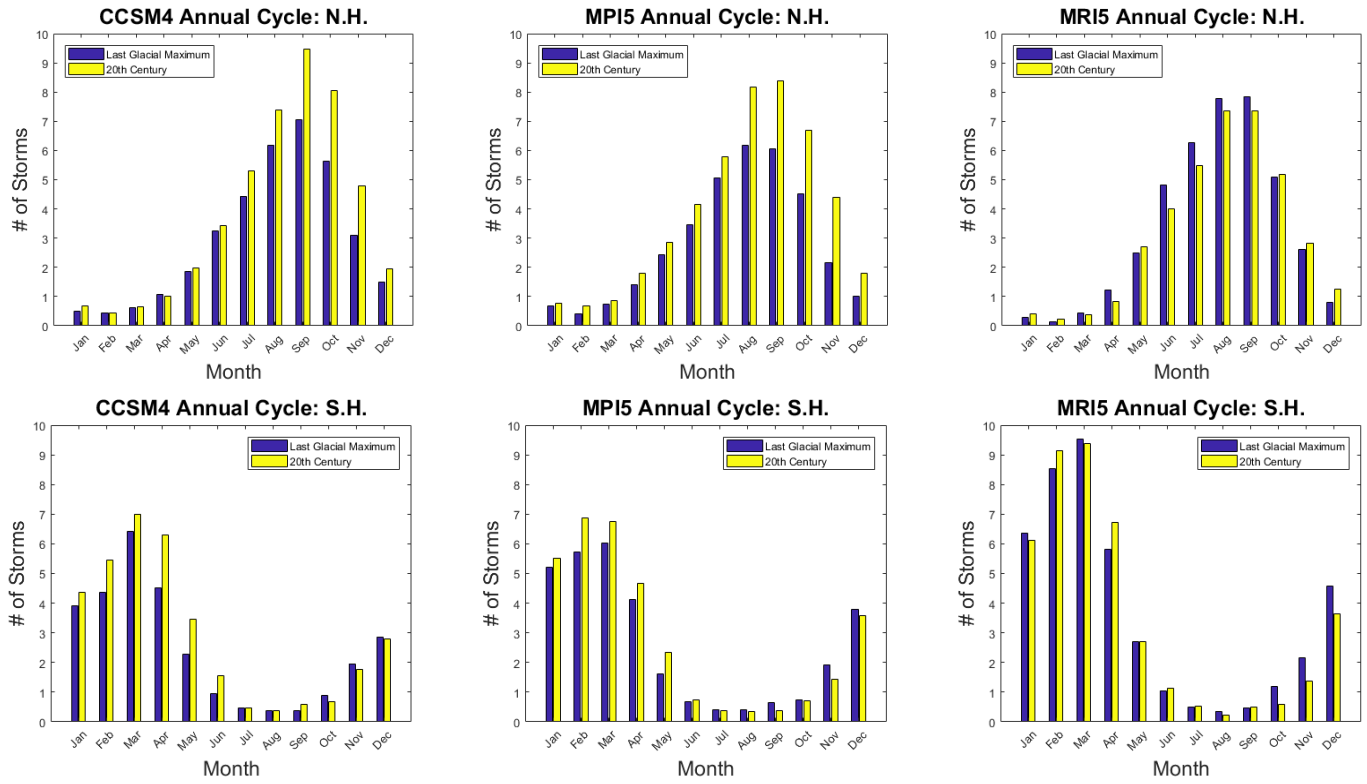

Figure 3- A comparison of annual cycle in both the Northern and Southern hemisphere. The top row depicts patterns in the Northern Hemisphere, whereas the bottom row depicts patterns in the Southern Hemisphere. In each row there are three graphs, one for each climate model, that depict the average annual cycle of downscaled TCs. The annual cycle of LGM climate states are represented in blue, while the annual cycle of 20th Century climate states are represented in yellow. Data was normalized to 80 storms per year for each simulation's 20th Century.

As the annual cycle for the LGM did not vary much from the 20th Century, we defined identical storm-season months for each. Henceforth, we define the Northern Hemisphere storm-season as the July-October months (JASO), and the Southern Hemisphere storm-season as the January-April months (JFMA).

General Basin Characteristics and Statistics

Basin-wide statistics were calculated for the primary region in the North Atlantic, with boundaries defined in Table 2 (see previous section). For all environmental parameters, the storm season average was used. As discussed in the introduction,wind shear and potential intensity are key indicators of TC favorability. A weighted combination of these values is used to calculate

storm-season average CGI, and all three are compared across climate states. Two basins were studied in detail- the Northern Atlantic Basin and the Western North Pacific. Comparisons were made between the LGM and 20th Century climate states for each model. Each basin is split into a "primary" and "secondary" formation region, which when analyzed together was referred to the "combined" region.

Basin Characteristics

In the Atlantic Basin, we present statistics for the combined Atlantic regions in lieu of each individual region. This is because the direction of intra-model changes in analyzed parameters did not change when combining both regions, and all basin-wide changes remained statistically significant. Incorporating both the primary and secondary region also increased the average CGI in both the CCSM4 and MRI simulations. From this we determined that the combined region was more representative of TC formation in the Atlantic than the primary region alone. Of course, this does not mean that the most significant changes take place in the secondary region compared to the primary region. Later discussion will elaborate on how many of the significant changes in environment conditions remain concentrated within the primary Atlantic formation region.

A comparision of average wind shear, potential intensity, and CGI characteristics is presented in Figure 4. Basin-wide significance results are displayed in Table 3. In the Atlantic combined region, both the CCSM4 and MPI simulations depict an LGM climate with increased average wind shear and decreased average potential intensity relative to the 20th Century control. These models also depict lower values of CGI during the LGM. Changes in all three parameters in the Atlantic combined region were determined to be statistically significant in the CCSM4 and MPI5 simulations, using a p-value threshold of 0.05. This indicates that environmental

conditions in the CCSM4 and MPI5 LGM were less favorable for TC development than their respective 20th Century climate state. In this case, TC favorability increased with warming climate.

Table 3

Was the Change in Atlantic Combined Region Average Values Statistically Significant?			
	CGI	**Potential Intensity**	**Wind Shear**
CCSM4	Yes	Yes	Yes
MPI	Yes	Yes	Yes
MRI	Yes	Yes	Yes

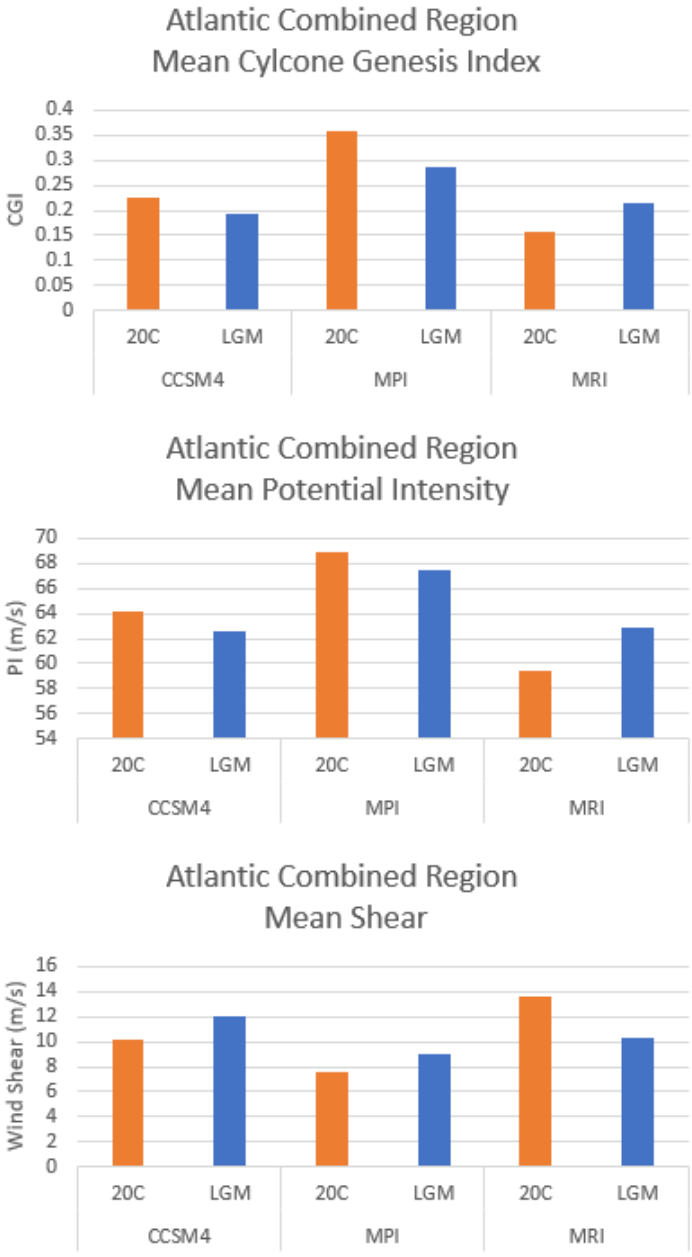

Figure 4- Comparision of mean environmental values within the Atlantic combined region during the Northern Hemisphere storm season (July-October). Averages taken during the 20th Century are displayed in orange, while averages taken during the LGM are displayed in blue. The first graph compares Cyclone Genesis Index (CGI), the second graph compares potential intensity (PI), and the third graph compares vertical wind shear.

In contrast to that of the CCSM4 and MPI simulations, MRI environmental characteristics within the Atlantic combined region were generally more favorable during the LGM as compared to it's 20th Century. During MRI's LGM, average wind shear in this region is

weaker and average potential intensity stronger. This resulted in larger values of CGI during the LGM, suggesting that this region has a more favorable environment during the LGM storm-season. As was the case for the other two models, these changes within the combined region were determined to be statistically significant. In this case, TC favorability decreased with warming climate.

In the Atlantic combined region, average CGI was higher for both climates states of MPI than for any other simulation. This was also true for the underlying components of CGI; MPI had the highest average potential intensity and lowest avearge wind shear in this region. The significance of this finding is questionable, however, as inter-model comparision presents a more nuanced chanllege that intra-model comparisions. Parameters that are controlled within model simulations- such as parameterization methods- are not preserved between models. Furthermore, the downscaling methodology used for this analysis diminishes the effectivity of direct model comparision. This is a result of using a set number of TCs for each climate state, which precludes the use of overall TC count and diminishes the value of direct comparisions of TC PDI and track density between models. Resultingly, it is difficult to confidently attribute a cause to differences in overall magnitude. While we do investigate the impacts of intemodel variations in atmospheric circulation, we will mostly defer from direct inter-model comparisions of downscaled TC data.

In the Pacific basin, two regions of interest were partitioned (see Table 2 in the previous section). Figure 5 displays a comparision of the statistics of mean CGI, potential intensity, and wind shear for each of these regions.

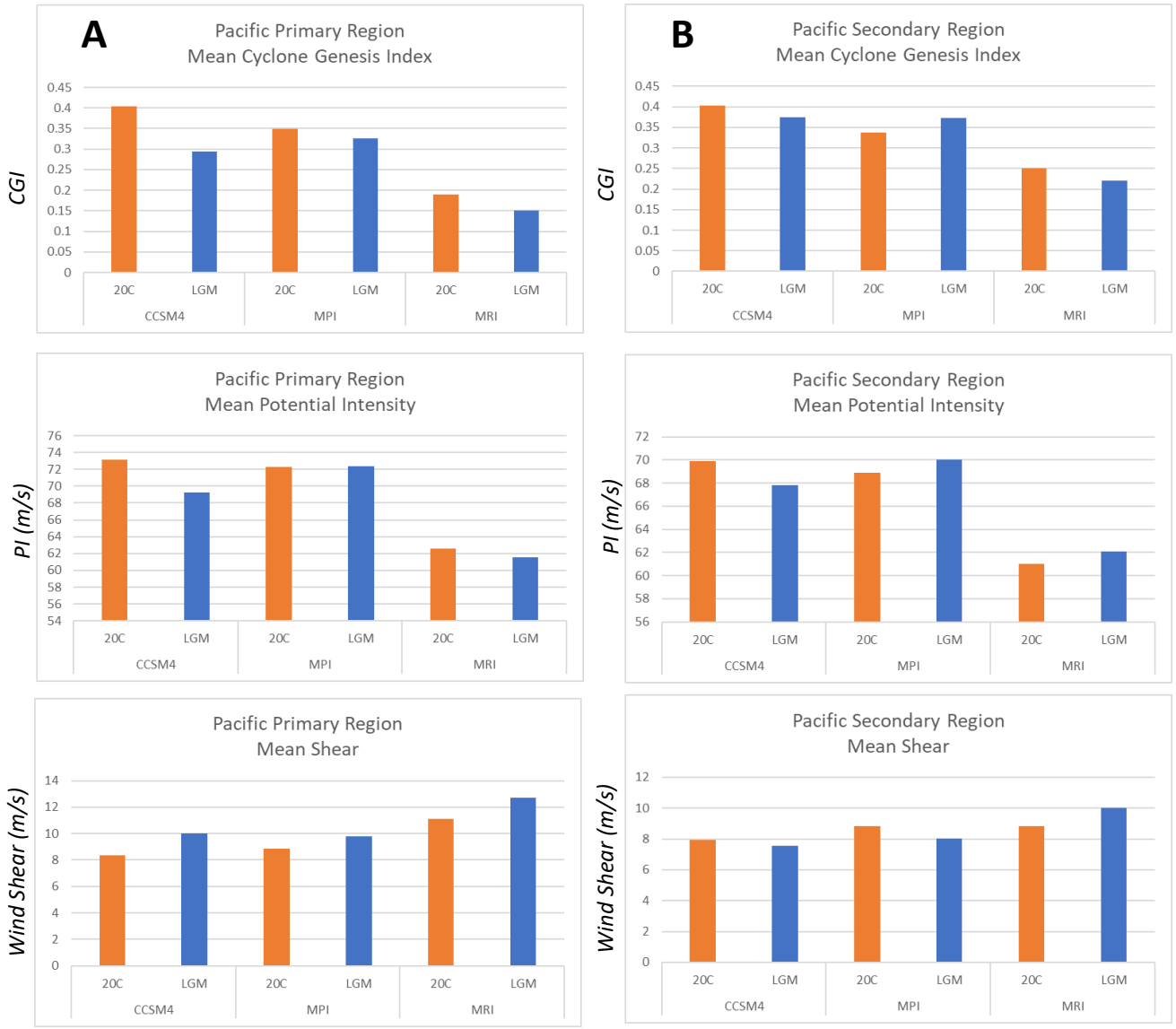

Figure 5- Comparision of mean environmental values for the Pacific primary and secondary regions. Averages are taken during the Northern Hemisphere storm season (July-October). Statistics for the primary region are displayed in the left column (A), and that of the secondary region are displayed in the right column (B). Averages taken during the 20th Century are displayed in orange, and averages taken during the LGM are displayed in blue. The first row compares Cyclone Genesis Index (CGI), the second row compares potential intensity (PI), and the third row compares vertical wind shear.

In the Pacific primary region, all three models show a relative decrease in CGI storm favorably for the LGM climate state. This decrease in overall favorably was found to be statistically significant for the CCSM4 and MRI model ($p<0.05$). CGI changes did not pass 95% significance for the MPI simulation using an unpaired two sample t-test.

Changes in potential intensity and wind shear were generally consistant with that of CGI for all three models in the Pacific primary region. One exception to this was the MPI model, which did not have a statistically significant change in PI (or CGI) between climate states. This likely contributed to the lack of significance in this model's CGI changes. Meanwhile, the CCSM4 did not experience a statistically significant change for wind shear in the Pacific primary region, significantly lower values of potential intensity during this region's LGM was enough to support a statistically significant change in CGI. A summary of statistical significance test results for the Pacific primary region is shown in Table 4.

Table 4

Was the Change in Pacific Primary Region Average Values Statistically Significant?			
	CGI	**Potential Intensity**	**Wind Shear**
CCSM4	Yes	Yes	Yes
MPI	No	No	Yes
MRI	Yes	Yes	Yes

The direction and significance of changes in the Pacific secondary region were more varaible than found to its west. Average parameters for this region are shown in the right column of Figure 5. Statistical analysis demonstrated a significant ($p < 0.05$) increase in the MPI depiciton of mean CGI during the LGM, and a significant ($p < 0.05$) decrease in the MRI depiciton of mean CGI during the LGM. Changes in CGI were not found to be statistically significant for this region in the CCSM4 model. Relatedly, there is a decrease in average wind shear and increase in average potential intensity for the MPI simulation's LGM climate. The exact opposite was true for the MRI simulation, with increased wind shear and decreased potential intensity during the LGM. All changes in potential intensity and wind shear were

determined significant in this region for the MRI and MPI simulations. Table 5 summarizes the significant test results for the Pacific secondary region.

Table 5

Was the Change in Pacific Secondary Region Average Values Statistically Significant?			
	CGI	**Potential Intensity**	**Wind Shear**
CCSM4	No	Yes	No
MPI	Yes	Yes	Yes
MRI	Yes	Yes	Yes

These results indicate that the utilized simulations show significant variability in the depiction of environmental change between the LGM and 20th Century. Higher average values of estimated TC favorabilty exist during the LGM for both the MRI Atlantic combined region and the MPI secondary Pacific region. Lower values of estimated TC favorability exist during the LGM for the CCSM4 Atlantic combined region, the MRI Atlantic combined region, the MRI Pacific secondary region, and the MPI Pacific secondary region. However, there exists the impact of arbitrary region boundaries. While static basin region boundaries are useful for interpretation, they are not robust to patterns and changes that encompass mutiple regions. To minimize errors and develop a more robust understanding of the changes occuring in each basin, we constructed spatial representations of enviornmental parameters and their calculated statistical significance.

Statistical Significance by Grid Point

In addition to calculating statistical significance for environmental changes within entire basins, it was also calculated at individual grid-points.This was done for changes in storm-season average CGI, potential intensity, and wind shear using an unpaired two sample t-test (this test is

discussed in detail in previous section). Figure 6 maps the statistical significance of CGI change within the Atlantic Basin. The primary and secondary basin outlines are overlain on the figure, in red and pink outlining, respectively. Similar- but not identical- patterns in statistical significance were seen for changes in PI and shear (not pictured).

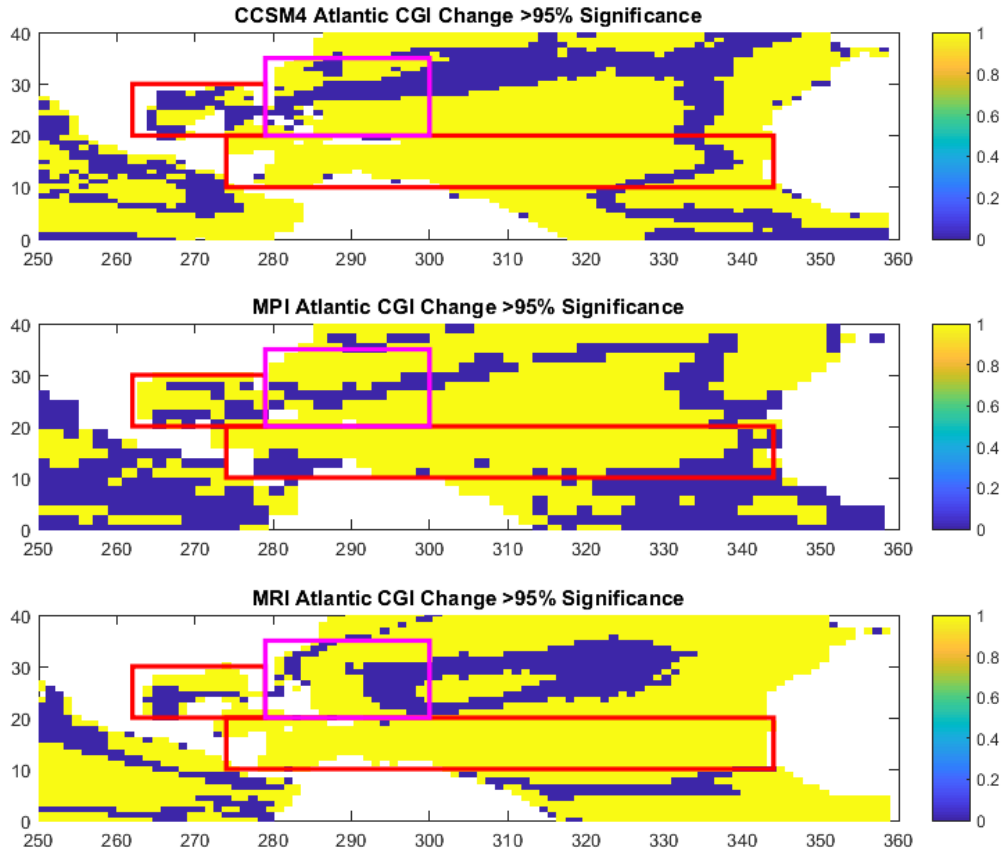

Figure 6- Spatial depiction of the statistical significance of LGM to 20th Century CGI changes in the Atlantic Basin based on an unpaired T-test (specifically described in the method chapter). Red boxes outline the Atlantic primary region, while the pink box outlines the Atlantic secondary region. Values of 1 indicate statistical significant changes in CGI, and values of 0 indicate regions where the null hypothesis could not be rejected.

In the Atlantic basin, all three simulations have broad regions of statistically significant CGI change in their Atlantic primary region, specifically in the open Atlantic and the southern Caribbean Sea. This distribution appears more sporadic within the secondary region and parts of the Gulf of Mexico. This suggests that environmental conditions within the primary region-

besides that of the Gulf of Mexico- likely had the most widespread impact on basin-wide TC favorability.

Figure 7 maps the statistical significance of CGI change within the Pacific Basin. Within the primary region, both the CCSM4 and MRI models depict a broad area of statistically significant CGI change. This is not true, however, for the MPI simulation. There, statistically significant changes in CGI are typically confined close to the continental margins and the central primary region is devoid of widespread change in CGI. These spatial distributions correspond well to Table 4, where MRI failed to pass a statistical significance test for CGI.

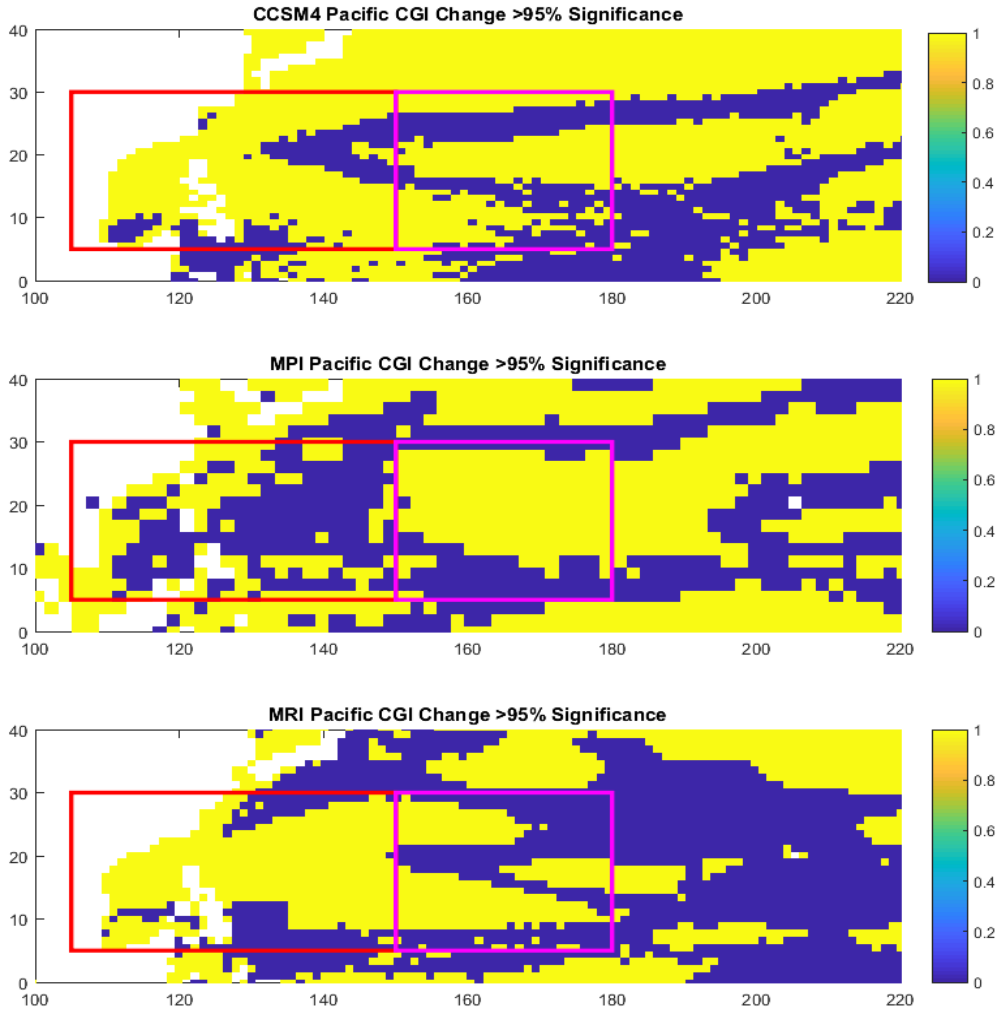

Figure 7- Spatial depiction of statistical significance of LGM to 20th Century CGI changes in the Pacific Basin based on an unpaired T-test (specifically described in the method chapter). The red box outlines the Pacific primary region, while the pink box outlines the Pacific secondary region. Values of 1 indicate statistical significant changes in CGI, and values of 0 indicate regions where the null hypothesis could not be rejected.

Statistically significant CGI change is less widespread in the secondary region for CCSM4 and MRI. There, both simulations have separated patches of significance. As will be discussed later, these separated patches corresponded to CGI changes in different directions. Having multiple regimes of CGI with the same region can complicate its overall average- hence the failure of the CCSM4 secondary region to pass a significance test. This is representative of

one of the complications arising from arbitrary region boundaries. Meanwhile, only MPI had a single broad area of significant CGI change located within the Pacific secondary region.

Spatial Comparisons of TCs to Environmental Factors

Spatial distributions of PDI were the primary metric used to assess trends in downscaled TCs across simulations and climate states. PDI was compared to spatial distributions of environmental parameters, including wind shear, potential intensity, and CGI. This allowed us to assess the relationship between environmental averages and downscaled TCs.

Northern Atlantic Basin

Figure 8 compares the Atlantic Basin total storm-season average of CGI between each simulation and climate state. Figure 9 compares the yearly summed PDI of downscaled storms between each simulation and climate state. Because average values were already compared for the overall basin, we are most interested in spatial trends within and just outside the previously analyzed primary and secondary regions. A land mask was used to remove undesired data points over land; however, artifacts of land-interaction can sometimes be seen at the boundaries of continents.

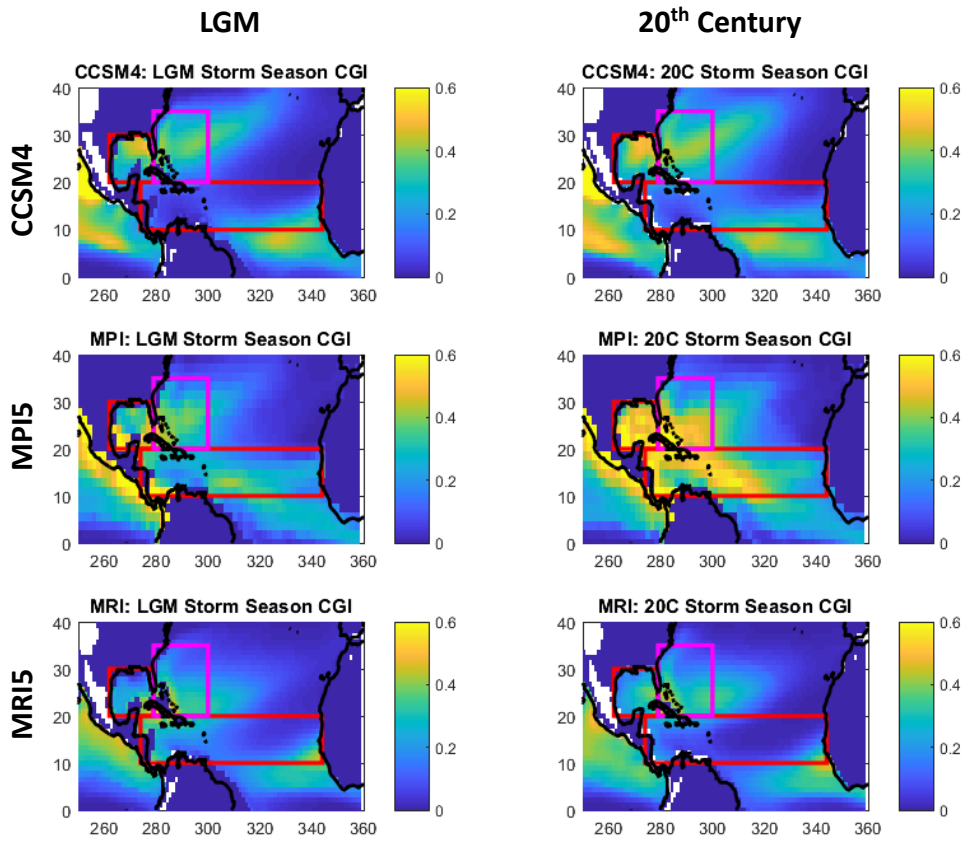

Figure 8- Spatial comparison of the storm-season average of CGI for each model and simulation. LGM climate states are plotted in the left column, and 20th Century climate states are plotted in the right column. Red boxes outline the Atlantic primary region, and the pink box outlines the Atlantic secondary region.

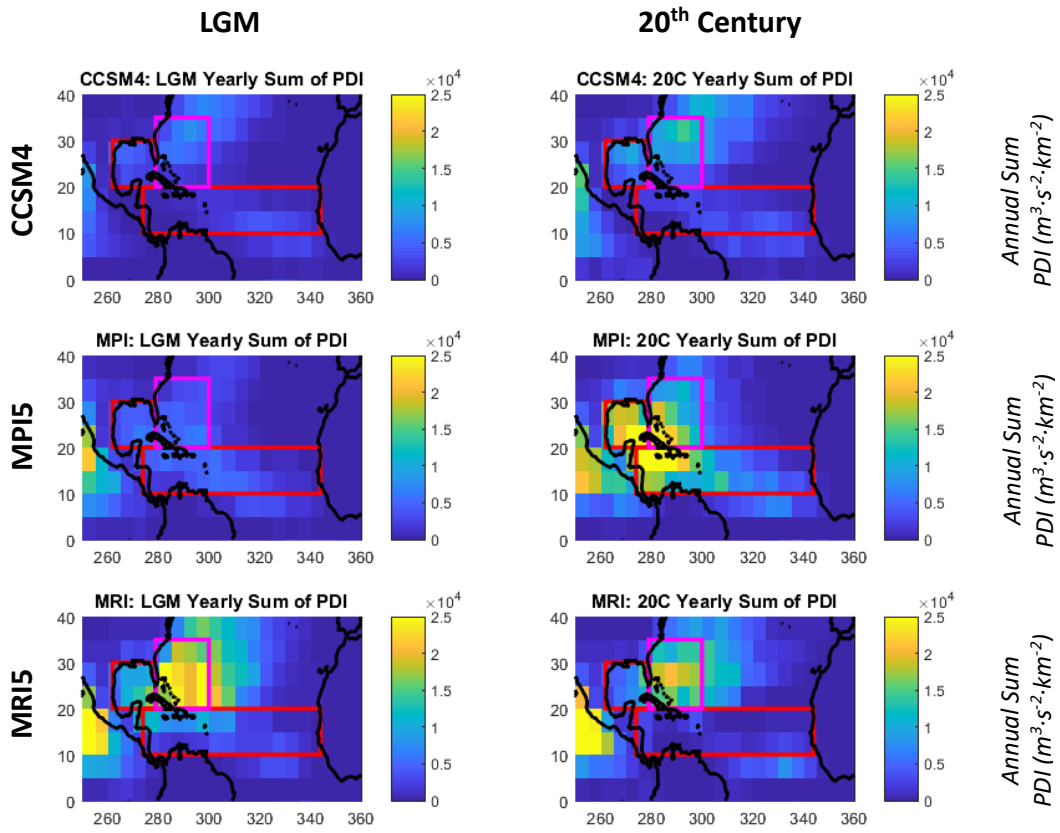

Figure 9- Comparison of the yearly summation of PDI (done grid-box by grid-box) for each model and simulation. LGM climate states are plotted in the left column, and 20th Century climate states are plotted in the right column. Red boxes outline the Atlantic primary region, and the pink box outlines the Atlantic secondary region.

In its 20th Century climate simulation, the MPI model generally produced higher values of PDI in the Atlantic than the other two models. Relatedly, MPI's CGI values in the Atlantic Basin were also the largest of all three models. The largest values of PDI for both the MRI model and CCSM4 simulations are concentrated outside of the "primary" formation region and instead located within the "secondary" formation region. In contrast, maximum values of CGI are often focused in the secondary region. This is likely due to the displacement of maximum TC intensity from their initial genesis point. If regions of large CGI are associated with high rates of TC formation, PDI maximums would be displaced downstream from CGI maximums as TCs

strengthen. Thus, changes in TC favorability for a certain location would likely impact PDI downstream.

In the Atlantic basin, a larger percentage area of statistically significant change was located within the primary region. This suggests that the primary region likely still has an important influence on downscaled TC characteristics, despite the displacement of maximum values of yearly summed PDI.

Figure 9 suggests that out of all three models, MRI downscaling produced the largest values of PDI during the LGM. However, differences in in the PDI of the CCSM4 and MPI, as well as the storm-season average CGI values from all three models, were not easily seen in the raw distributions. These plots also do not precisely depict changes from the LGM to the 20th Century climate state.

To better quantify the impact of the differences in LGM and 20th Century climate on parameters such as PDI and CGI, anomalies were calculated between each model's climate state. For this method we consider the 20th Century as a model's control state and display deviations in LGM climate characteristics. This was calculated grid-box by grid-box, using storm-season averages. PDI is an exception, with differences in the yearly summation of PDI used instead.

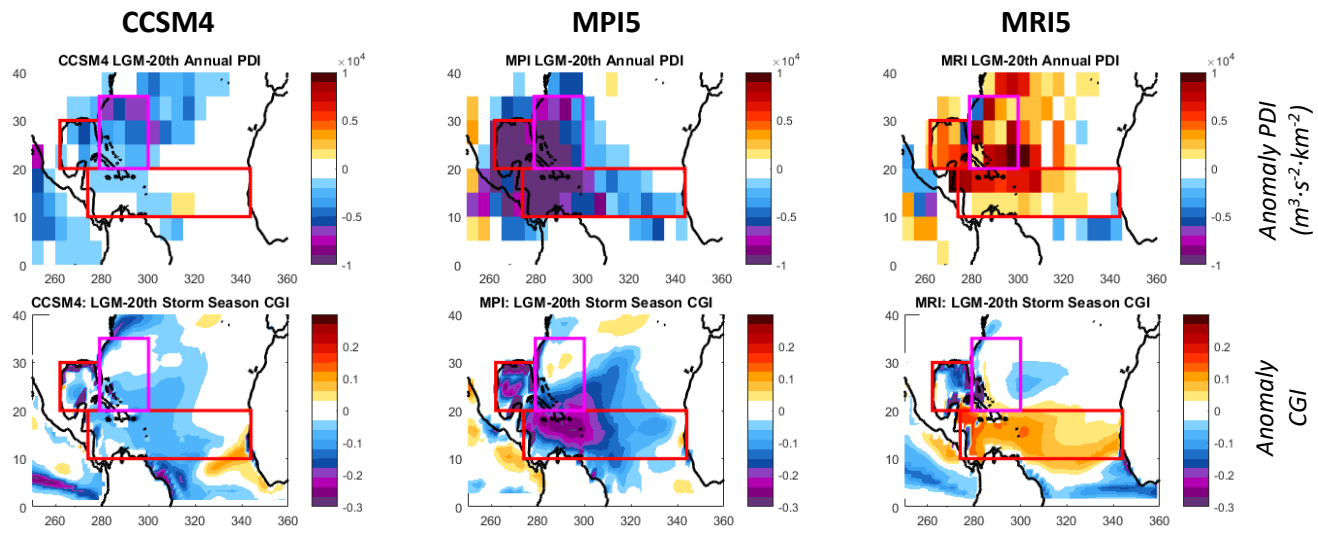

Figure 10- This figure depicts the PDI and CGI anomaly for the LGM compared to the 20th Century in the Northern Atlantic basin. Row 1 displays changes in annual PDI, while Row 2 displays changes in storm-season average CGI. Three models are plotted in each. Cool colors represent negative anomalies, while warm colors represent positive anomalies. Red boxes outline the primary Atlantic regions- pink outlines the secondary Atlantic region.

Figure 10 compares the spatial distribution of LGM anomalies in annual summed PDI and storm-season CGI. Warmer colors indicate higher values of PDI/CGI during the LGM for a given grid box, and cooler colors depict lower values. Both the CCSM4 and the MPI model depict overwhelming decreases in Atlantic PDI during the LGM- with MPI model depicting a more intense decrease in PDI than the CCSM4. Meanwhile, the MRI model is an outlier with generally higher values of PDI during the LGM. This decrease in PDI with warming climate depicted in the MRI Atlantic basin conflicts with the consensus on TC intensity response found in previous work, as discussed earlier (e.g. Bender et. al. 2010, Murakami et. al. 2012, Sobel 2016). However, trends within a specific region are not always indicative of the entire globe.

As is shown in Figure 10, changes in CGI favorability positively correlated with changes in the PDI of downscaled storms for all three model depictions of the Atlantic basin. Both the CCSM4 and MPI5 models depict large scale decreases in CGI during the LGM, with larger amplitude decreases in MPI5 compared to the CCSM4. MRI is again the outlier here, with

widespread increases in CGI during the LGM compared to the 20th Century. Despite their general alignment, changes in CGI and PDI are slightly displaced for all three simulations. Where they do not overlap, bands of positive/negative anomaly in CGI are generally concentrated to the south of corresponding changes in PDI. A possible explanation for this behavior is the typical displacement of maximum TC intensity from initial genesis point.

In all three simulations, the largest changes in CGI typically occurred within the southern primary formation region, outlined in red. The secondary region typically contained lower magnitude changes, and even changes in in the opposite direction from that of the primary region. This was especially true for the MPI and MRI simulations, while the CCSM4 had more uniform changes across both regions. For the most part, changes in CGI were similar in direction across the majority of the primary region. A major deviation from this is found in the MRI simulation, where the Gulf of Mexico saw greatly reduced CGI during the LGM while the rest of the primary region saw a large increase.

For all three simulations, changes in the 10°N-20°N Atlantic environment appear to have the greatest impact on downscaled storms. For example, most of the MRI region demonstrates increased PDI during the LGM, with the greatest changes in CGI occurring in the 10°N-20°N portion of the primary region. This relationship generally holds true for the other two simulations and is supported by our previous analysis of Figure 6, where the 10°N-20°N region of the Atlantic saw the highest percentage of statistical significance of any region in the Atlantic.

As discussed earlier when introducing CGI, the two underlying atmospheric components contributing to this metric is potential intensity and 250-850mb wind shear (refer to Equation 2). Identifying where and by how much these components change with warming can aid in identifying their underlying origin, especially in terms of global circulations. Figure 11 depicts

the LGM anomaly of storm-season average wind shear and potential intensity. Changes in relative sea-surface temperature (RSST) are also depicted. RSST is defined as the deviation of a grid point's SST from the 30°S-30°N (tropical) average.

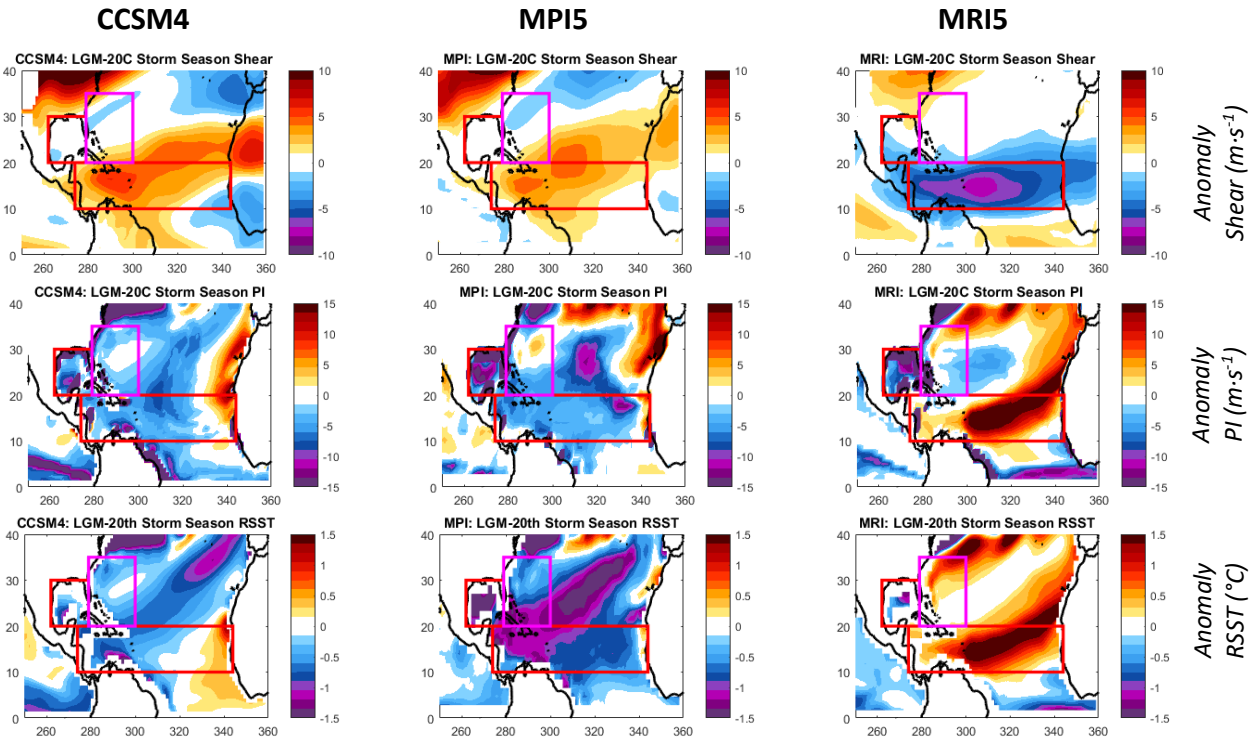

Figure 11- Comparision of LGM anomaly storm-season averaged 850-250 mb vertical wind shear, potential intensity, and relative sea-surface temperature for each simulation in the North Atlantic basin. 20th Century values are used as the control. RSST is the deviation of SST from the tropical (30S-30N) SST average. The primary Atlantic region is boxed in red, the secondary region is boxed in pink. Larger values of vertical wind shear generally has a detrimental effect on TCs, while larger values of potential intensity and RSST generally indicate a more favorable environment for TCs.

In the CCSM4 simulation, there was typically a positive 1 to 5 m/s LGM anomaly in wind shear and a negative 2 to 10 m/s LGM anomaly in potential intensity. Changes in wind shear are concentrated within and slightly to the north of the primary box located from 10°N-20°N. Changes in PI, meanwhile, are more evenly spread across the entire Atlantic basin and Gulf of Mexico. This combination conspires to reduces the average total amount of energy available to TCs while increasing the entrainment of low entropy air through wind shear,

resulting in a less conducive environment for TC intensification during the LGM. These environmental modifications are likely the cause of the generally reduced TC PDI during the CCSM4 LGM. This is not exclusively true across the basin. One exception is a plume of positive PI and reduced wind shear located off the west African coast during the CCSM4 LGM. This area is also visible in Figure 10 as an area of slightly increased CGI. Heightened TC favorability in this region may have contributed to the positive LGM anomaly in PDI for one square of the Central Atlantic. However, the impacts of this change are minimized by the overall lack of favorability for TC development in this region.

The MPI model had similar changes of storm-season average PI and wind shear as that of the CCSM4. In this model's simulation of the LGM, negative CGI anomalies can be tied to reduced PI and increased wind shear. This results in a less favorable environment for TCs during the MPI LGM, likely resulting in the diminished PDI shown in Figure 10. In the MRI model, changes in shear and PI were effectively flipped in comparison to the CCSM4 and MPI. In the MRI's depiction of the Atlantic primary region, wind shear was on average 5 to 10 m/s lower during the LGM storm season. This same region of the Atlantic had average increases in PI of 5-10 m/s. This results in greater average TC favorability- represented by CGI- across most of the Atlantic Basin, potentially leading to the corresponding increases in downscaled TC PDI.

Figure 11 also depicts the LGM anomaly of storm-season average RSST in the third row. RSST has been shown in modeling and observational studies to be a better proxy for PI than absolute SST as it more readily considers changes in upper-troposphere thermodynamics (Vecci and Soden 2007, Ramsay and Sobel 2010). This relationship is shown in these simulations of the Atlantic Basin, where changes in RSST behaved similarly to changes in PI. Both the CCSM4 and MPI models had generally decreased RSST during LGM for most of the basin regions, while

the MRI model was again the outlier with generally increased RSST during the LGM. For the MRI model, this increased RSST was mostly concentrated in the Atlantic primary region (excluding the Gulf of Mexico).

Spatially, changes in the storm-season averages of CGI, PI, and shear aligned excellently with corresponding changes in downscaled tropical cyclone PDI. However, two different solutions for TC activity in the LGM Atlantic basin arose. One, as represented by the CCSM4 and MPI models, suggests stronger wind shear and less favorable thermodynamic characteristics made the LGM much more hostile to TCs than the 20th Century. The MRI model, however, implies that the LGM Atlantic basin could have been more favorable for TC development and intensification. To better understand the reasons for this variability, a broader understanding of the underlying atmospheric circulation patterns and their changes in each model was necessary.

To understand how atmospheric wind patterns influenced vertical wind shear in the Atlantic basin, we next analyze storm-season average 250mb and 850mb wind patterns for each model's simulated climate states. These were compared to wind shear to estimate their relative contribution. In general, changes in 250mb wind speed and direction were more directly related to changes in wind shear than the winds at the 850mb level within the Atlantic Basin. Thus, here we choose to display depictions of 250mb level winds in lieu of those at the 850mb level.

Figure 12 depicts the storm-season average wind shear for each model's LGM and 20th Century simulation. Figure 13 depicts storm-season average 250mb wind speed and direction for each model's LGM and 20th Century simulations.

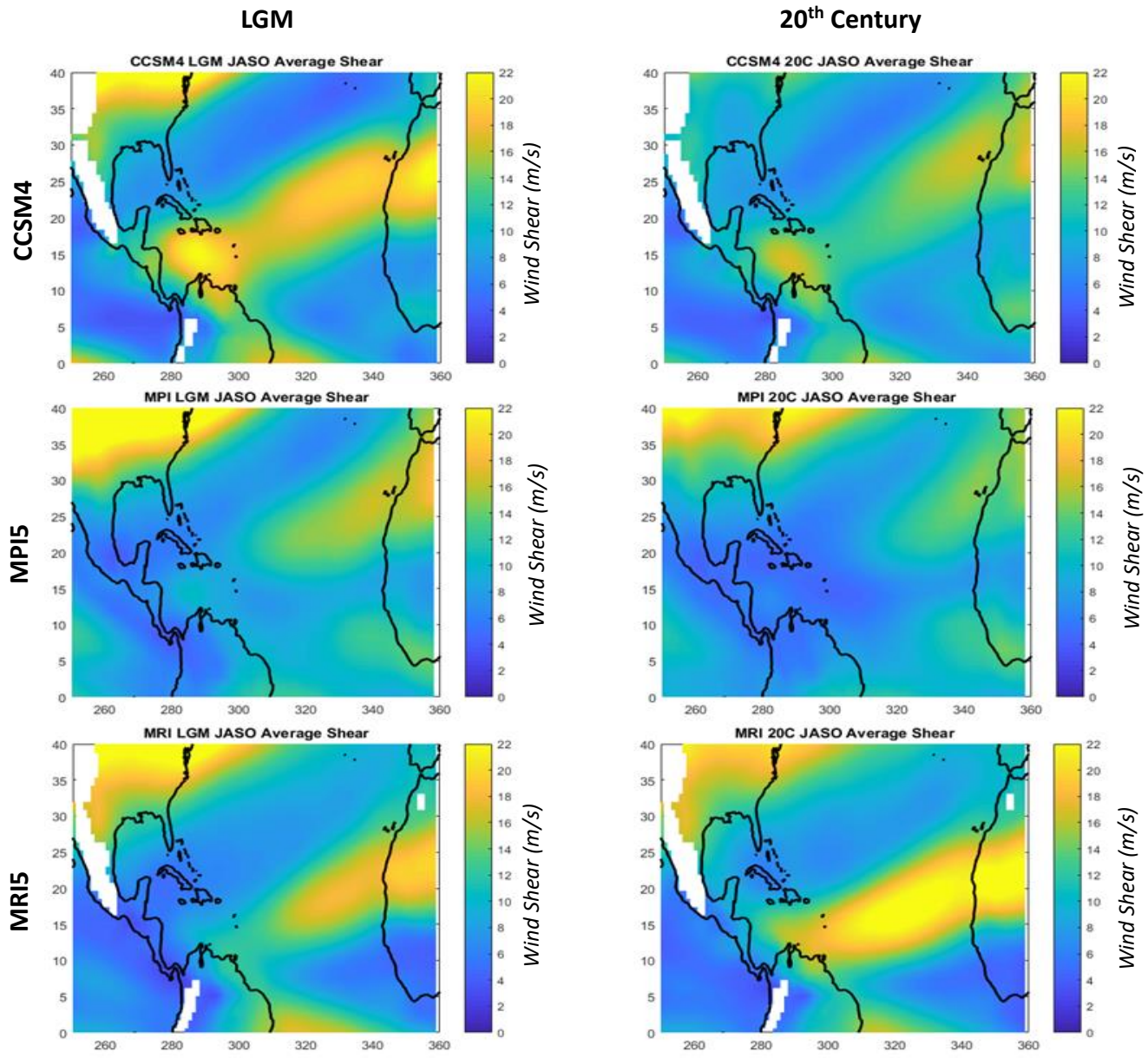

Figure 12- Simulation and climate state comparision of storm-season average wind shear in the Atlantic Basin. Units are m/s.

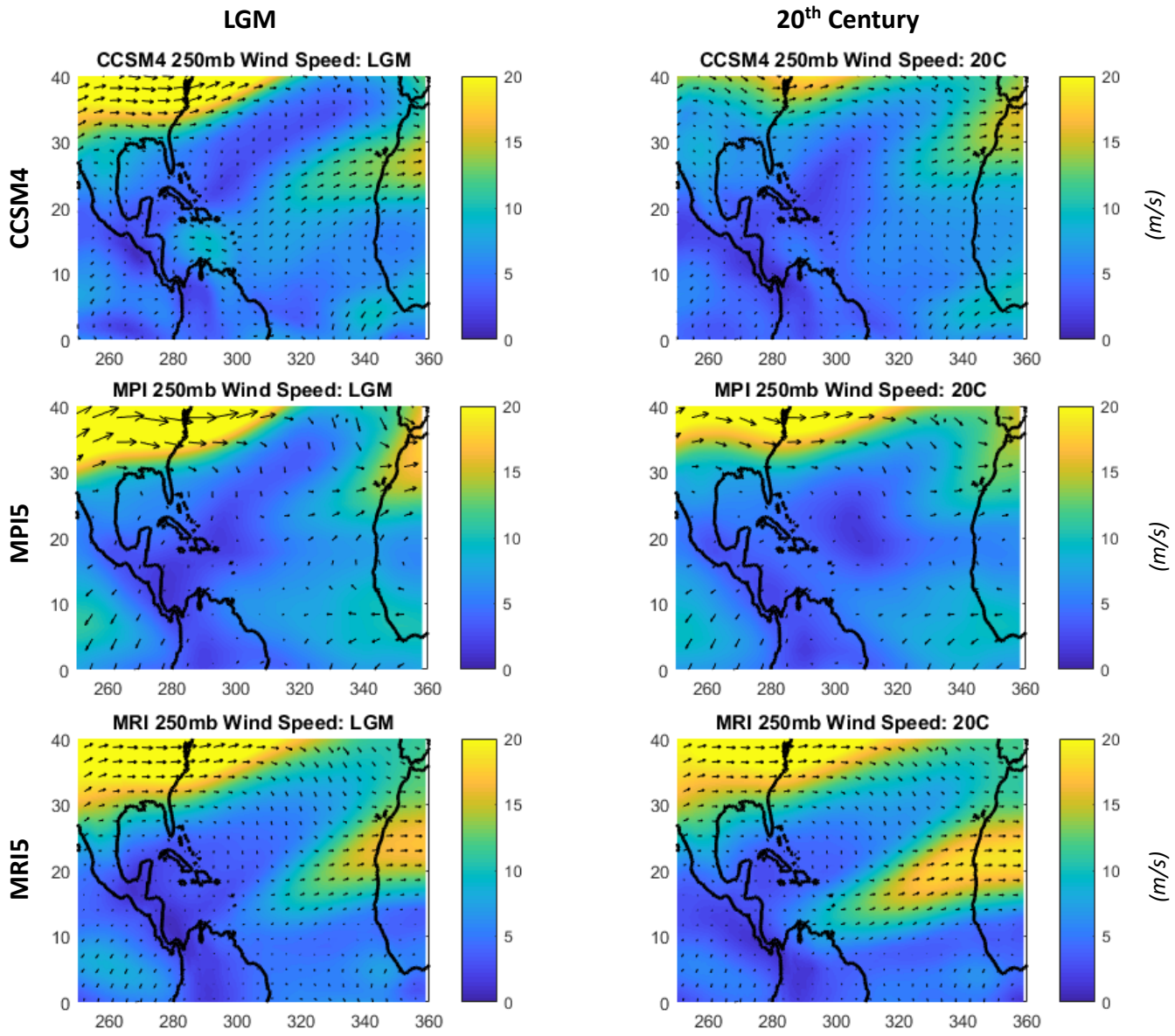

Figure 13- Simulation and climate state comparision of storm-season avearge 250mb wind speed and direction. Shaded contours are of the absolute magintude of average wind speed, and plotted vectors show the average 250mb wind direction. Units are m/s.

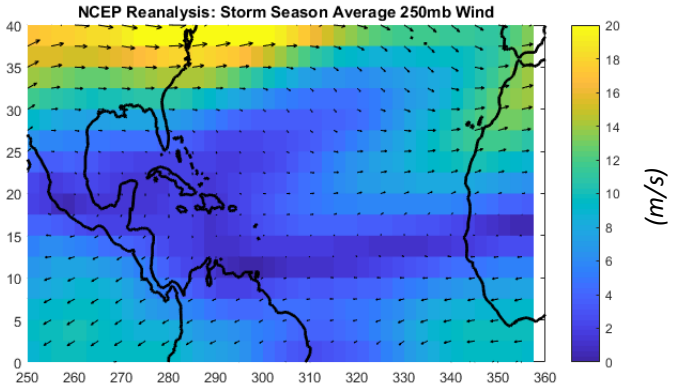

Figure 14- Climatological average storm-season 250mb wind speed and direction from 1948-2017. Wind is shaded in m/s. NCEP Reanalysis data provided by the NOAA/OAR/ESRL PSD, Boulder, Colorado, USA, from their Web site at https://www.esrl.noaa.gov/psd/. Further information can be found in Kalnay et. al. (1996).

MRI differs from the other two models in its depiction of a strong sub-tropical jet over Africa in both the LGM and 20th Century simulations. This jet appears to have a significant impact on environmental wind shear in the Atlantic, as shown in Figure 12. While this deviation is clear when comparing simulations of the 20th Century, it should be noted that this subtropical jet is stronger and further south for the MRI model even when just comparing the LGM.

Analysis of average 250mb wind vectors and circulation patterns- along with comparisons to the 850mb level- suggests that wind shear is most strongly influenced by the 250mb winds in all three models. As previously discussed, the MRI model shows generally decreased values of storm-season average wind shear during the LGM compared to its 20th Century (Figure 11). This change in wind shear aligns with a weakened sub-tropical jet during the LGM.

Shifts in the sub-tropical jet (and relatedly, wind shear) could be the result of variations in temperature gradients over the African continent. If this is the case, we would expect to see sharper temperature gradients during both MRI climate states as compared to the other models.

Further work in this area- both on confirming the existence of these temperature gradients and understanding why they may deviate between models- is ongoing.

Despite its anomalous change with warming, the MRI simulation depicts similar magnitudes of wind shear during the LGM (see Figure 12) in comparison to the other two simulations. This is true for the majority of the Atlantic Basin, where MRI LGM wind shear magnitude is generally similar to that of the CCSM4 simulation and is slightly larger than that of the MPI simulation. Only during the 20th Century simulation does MRI wind shear becomes an outlier. There, the sub-tropical jet stream and resulting wind shear are significantly stronger for the MRI than the other two models. Additionally, the MRI depiction of the 20th Century sub-tropical jet significantly deviates from the NCEP re-analysis 20th Century climatology, shown in Figure 14 (Kalnay et. al. 1996). CCSM4 and MPI compare much more reasonably to the observed climatology.

A portion of the mid-latitude jet stream is visible over the North American continent from 30°N-40°N, and all three models depict a stronger mid-latitude jet in the graphed region during the LGM. This region is outside of the maximum values of TC PDI in the Atlantic, and thus its direct impact on TC characteristics could not be directly quantified in this basin. We hypothesize that this southern shift and/or intensification of the mid-latitude jet stream likely did not have a direct effect on downscaled TCs confined to the tropical latitudes of the Atlantic. However, a stronger mid-latitude jet stream could certainly impact TCs reaching higher latitudes, and indirectly influence basin favorability through other means. This area requires a more direct analysis for more conclusions to be made.

In the Atlantic basin, deviations in the MRI model's 20th Century characteristics had extensive ramifications on comparisons to other models, making portions of the Atlantic storm

environment much more hostile than it would have been otherwise. This highlights one of the drawbacks of utilizing a comparative methodology. Considering the large errors in the MRI's 20th Century climate depictions, the solution offered by CCSM4 and MPI seems much more reliable in the Atlantic basin.

Western North Pacific Basin

In this section, the "primary region" and "secondary region" are areas defined for the Western North Pacific in Table 2 (see previous section). Figure 15 compares this basin's total storm-season average of CGI for each model and climate state, and Figure 16 does the same for yearly summed TC PDI. The red box overlain on provided figures outlines the Pacific primary region, while the pink box outlines the Pacific secondary region. For both the CCSM4 and MPI simulations, the highest concentration of annual PDI is located within the primary region- with some overlap into the secondary region. This was true for both climate states, although CCSM4 showed a pronounced shift of PDI to the west for its 20th Century simulation as compared to that of the LGM. Within the MRI simulation, PDI was mostly concentrated within the secondary region and near the eastern boundary of the primary region. Already this suggests major differences in the TC formation region of the MRI model compared to that of the CCSM4 and MPI.

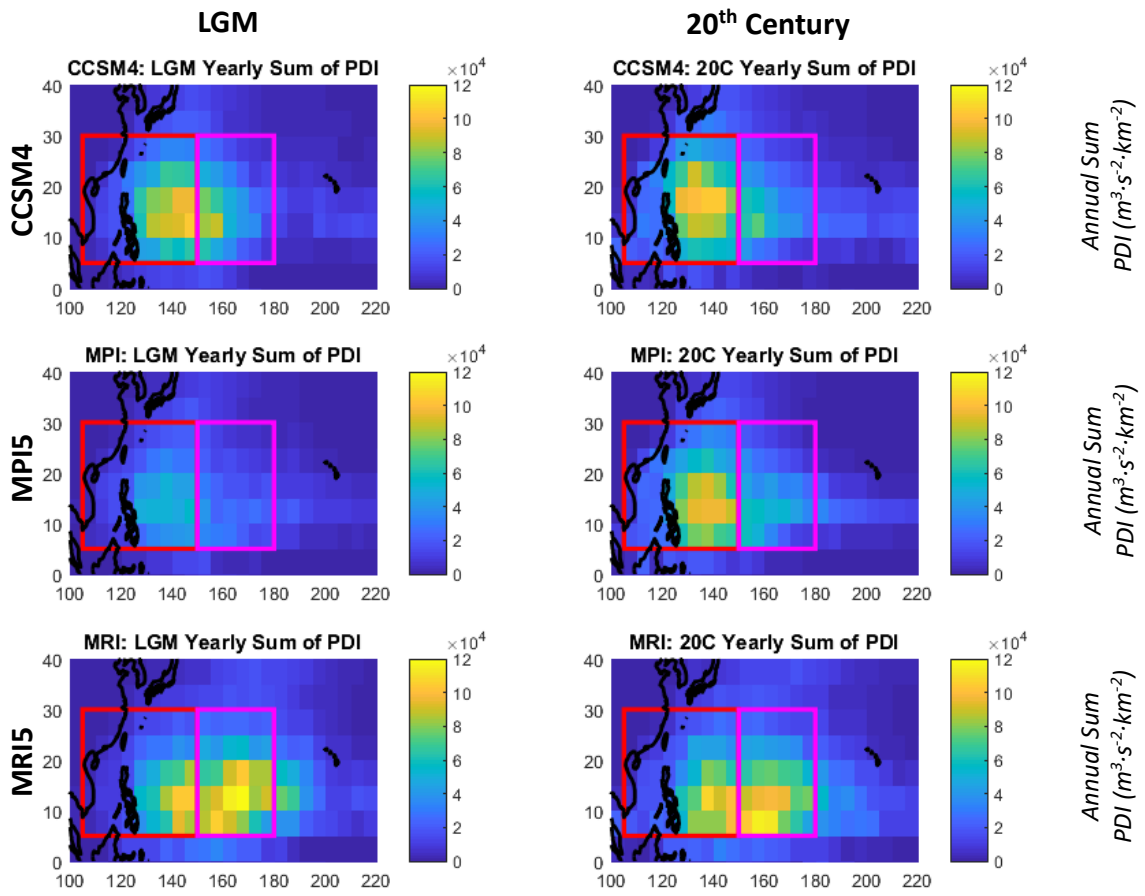

Figure 15- Comparison of the storm-season average of CGI for each simulation and climate state in the Western North Pacific Basin. The Northern Hemisphere storm-season of July-October was used for averaging. LGM climate states are plotted in the left column, and 20th Century climate states are plotted in the right column. The red box encloses the Pacific primary region, and the pink box encloses the Pacific secondary region.

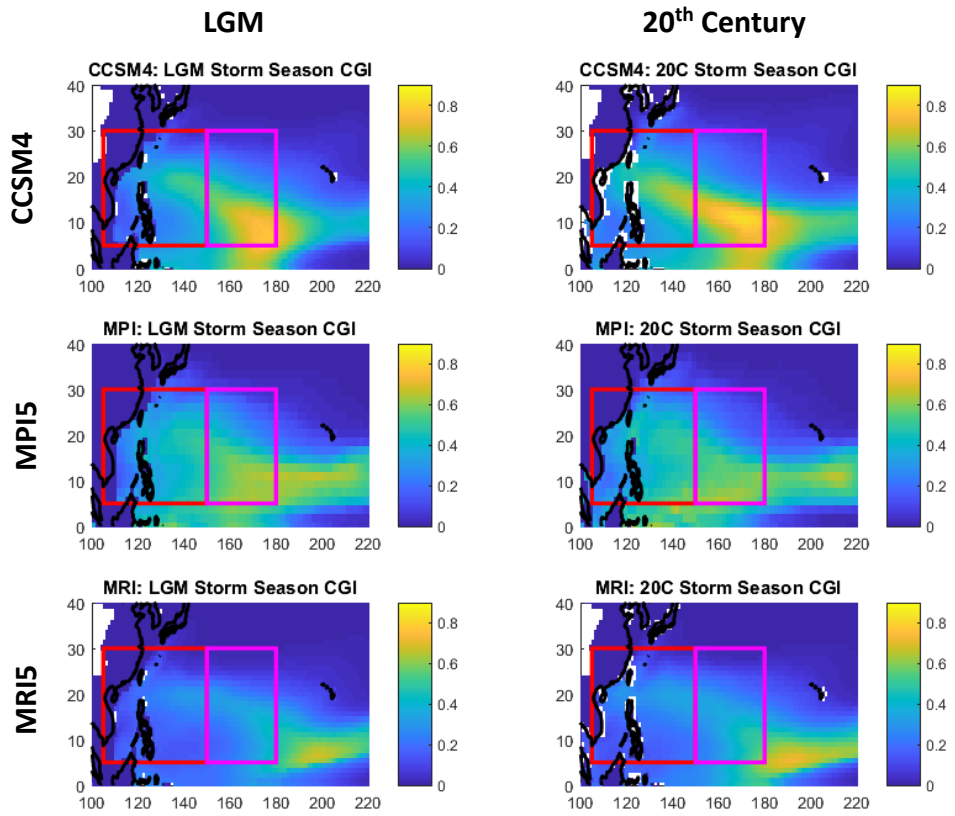

Figure 16- Comparison of the yearly summation of PDI (done grid-box by grid-box) for each simulation and climate state in the Western North Pacific Basin. The Northern Hemisphere storm-season of July-October was used for averaging. LGM climate states are plotted in the left column, and 20th Century climate states are plotted in the right column. The red box encloses the Pacific primary region, and the pink box encloses the Pacific secondary region.

As shown in Figure 16, both the CCSM4 and MPI simulations have the greatest TC favorability- as represented by storm-season CGI- within the secondary region. However, CGI values equal or greater than 0.4 stretch well into the primary region. As was seen in the Atlantic region, areas of maximum CGI were displaced from that of downscaled PDI.

The MRI model has its highest concentrations of CGI well to the east of either defined region in both climate states. Its values of CGI are generally lower within the primary region than in the other two models, and changes between MRI climate states are not easily discernable in Figure 16. MRI's highest values of PDI are also well to the east of the other simulations for both climate states. This suggests a fundamental difference in the MRI representation of

environmental conditions in comparison to the other two models, as was discovered for the Atlantic basin.

Figure 17 compares LGM anomaly yearly PDI with LGM anomaly storm-season CGI. An eastward displacement of CCSM4 PDI during the LGM- as could be seen in Figure 16- is depicted for this model. This shift corresponds with a general east-to-west shift in CCSM4 CGI with warming.

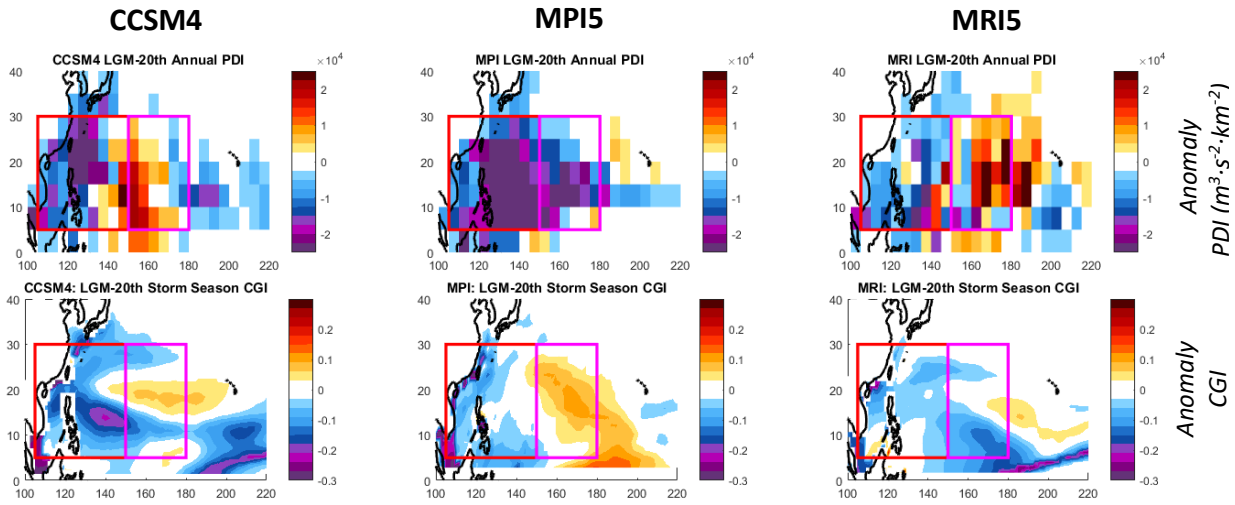

Figure 17- This figure depicts the PDI and CGI anomaly for the LGM compared to the 20th Century in the Western North Pacific Basin. The Northern Hemisphere storm season of July-October was used for averaging. Row 1 displays changes in annual PDI, while the second row displays changes in storm-season average CGI. Three models are plotted in each. Cool colors represent negative anomalies, while warm colors represent positive anomalies. The red box outline the primary Pacific region, while the pink box outlines the secondary Pacific region.

All three models portray reduced PDI (negative anomalies) for their LGM climate state as compared to the control. The CCSM4 and MRI models also depict a corresponding increase in PDI in the secondary region, suggesting TC activity moved westward as a result of LGM to 20th Century warming. The MPI model mostly lacked this shift, with widespread reductions in PDI across the entire basin during its LGM climate.

For the MPI model, a dramatic reduction in PDI across the entire basin is shown for its LGM climate state. This corresponds to relatively mild decreases in LGM storm-season CGI in the primary region and increases in CGI for the secondary region. Interestingly, statistical significance was spatially weak (mostly with $p>0.05$) within the primary region, and its region-wide T-test did not reject the null hypothesis (refer to Figure 7 and Table 4). The secondary region, meanwhile, had strong spatial depictions of significance and passed its region-wide T-test; in this case, the secondary region showed elevated CGI favorability for its LGM climate state. These results lay inconclusive the exact cause of MPI's shift in PDI, and multiple possibilities exist. For one, CGI only takes into consideration potential intensity and vertical wind shear, with inflexible weights assigned to each. Assuming constant weighting in all climates neglects the possibility that the sensitivity of downscaled TCs can vary for each parameter. TCs downscaled from the MPI region may also have been sensitive to other parameters not directly considered in CGI, resulting in a metric that is less representative of the residual environment within each model. Additionally, the major increases in LGM CGI lie at the fringe of the typical formation and favorability region shown in Figures 15 and 16, which could reduce its overall impact on downscaled TCs. Nevertheless, the lack of widescale statistical significance prevents us from reaching many definitive conclusions on the MPI simulation's depiction of Western North Pacific basin TCs.

The MRI simulation generally depicts a suppression of PDI in the primary pacific region and an enhancement of PDI in the secondary region during its LGM. An increase in PDI is also visible well to the east of both defined regions. Similar spatial patterns exist in CGI, although anomalies of CGI are shifted slightly to the east of corresponding anomalies in PDI. This leads to statistically significant decreases in LGM CGI in the secondary region, despite positive changes

in PDI for the same area. This appears to be another case of the displacement of CGI influence on PDI; reduced CGI in the secondary region most directly suppresses PDI in the primary region, while a plume of elevated LGM CGI to the east of the secondary region appears to most directly affect its PDI anomaly.

As was done in the Atlantic basin, PI, wind shear, RSST, and 250mb wind vectors were analyzed to determine their relative influence on CGI and environmental TC favorability. Figure 18 depicts the LGM anomaly of storm-season average wind shear, potential intensity, and RSST in the Pacific basin.

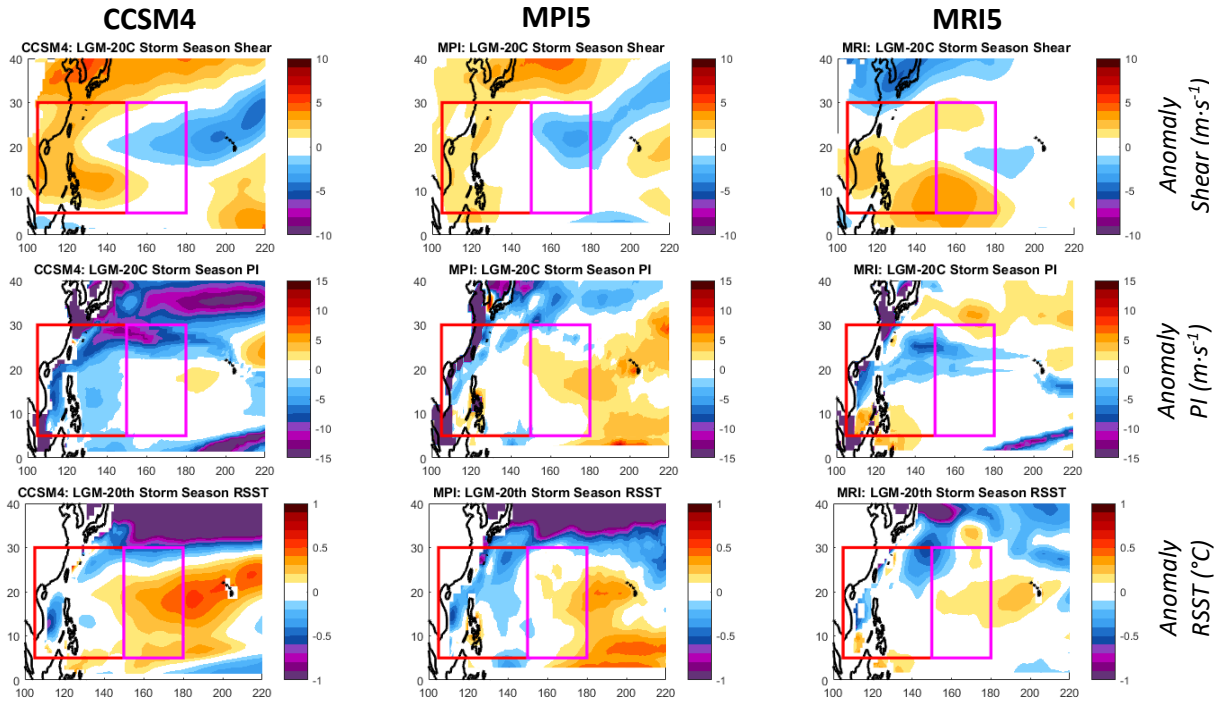

Figure 18- Comparision of LGM anomaly storm-season averaged 850-250 mb vertical wind shear, potential intensity, and relative sea-surface temperature for each simulation in the Western Pacific basin. 20th Century values are used as the control. The Northern Hemisphere storm season of July-October was used for averaging. RSST is the deviation of SST from the tropical (30S-30N) SST average. Larger values of vertical wind shear generally has a detrimental effect on TCs, while larger values of potential intensity and RSST generally indicate a more favorable environment for TCs. The primary Pacific region is boxed in red and the secondary region is boxed in pink.

In the CCSM4 LGM simulation, wind shear is enhanced relative to the 20th century control in the primary region and along the continental boundary. Suppressed values of LGM wind shear are observed in the secondary region, stretching into the Central Pacific from 15°N-25°N. LGM potential intensity is enhanced within the primary region and along the continental margin. This pattern correlates well with calculated CGI and explains the enhancement of LGM PDI within the CCSM4 primary region. Meanwhile in the secondary region. potential intensity was only modestly higher during the LGM. This, however, was still coupled with reduced wind shear, resulting in enhanced LGM CGI favorability and PDI. Elsewhere in the basin, large reductions in LGM potential intensity within the northern fringe of defined regions were largely too far north to have a pronounced impact on downscaled TCs. This is primarily due to the already low rates of TC formation in this part of the basin for both climate states. More work is needed to determine if this had a direct impact on the latitudinal extent of TCs.

PI and wind shear anomalies within the MPI simulation behaved similarly to that of the CCSM4, with minor differences in magnitude. As in the CCSM4, enhanced wind shear and suppressed potential intensity within the primary region and along the continental margin largely results in the diminished PDI of downscaled storms during the LGM. In the secondary region, the slight intensification of LGM potential intensity was coupled with reductions in wind shear. This translated to a large plume of increased CGI. However, as discussed earlier, PDI was still largely reduced in this region. In this case, shear and potential intensity do not appear to fully explain changes in MPI PDI for this region.

The MRI simulation differed significantly in its spatial distributions of wind shear and potential intensity. Like other simulations, its primary region contained reductions in potential intensity and stronger wind shear during the LGM, explaining reductions in LGM CGI and PDI.

However, enhanced LGM wind shear extends further to east than in CCSM4 and MPI, with only a small region of minimally decreased wind shear present in the Central Pacific. Furthermore, potential intensity increases during its LGM were largely confined to regions north of the primarily TC formation regions and along the continental margin from 2°N-10°N. This appears to shift TC PDI eastward during the LGM, into and beyond the secondary region. There, reductions in LGM wind shear and largely unchanged PI appear to increase the favorability of LGM TCs, as represented by CGI anomaly.

The third row of Figure 18 depicts the LGM anomaly of RSST for each simulation. Changes in RSST were directional aligned with changes in potential intensity for all three models. Unlike in the Atlantic, however, the magnitude of RSST changes were not as strongly linked to changes in potential intensity. The direct cause for this deviation is currently unknown.

As was the case in the Atlantic basin, one of the primary modulators for TC favorability was 250mb-850mb vertical wind shear. In the Pacific, changes in 250mb wind patterns somewhat corresponded to changes in wind shear but fail to completely explain its change across climate states. Figure 19 depicts a comparison of LGM anomaly 250mb wind speed and storm-season average wind vectors for each simulation. The 20th Century climatology of storm-season average from NCEP reanalysis is shown in Figure 20 (Kalnay et. al. 1996).

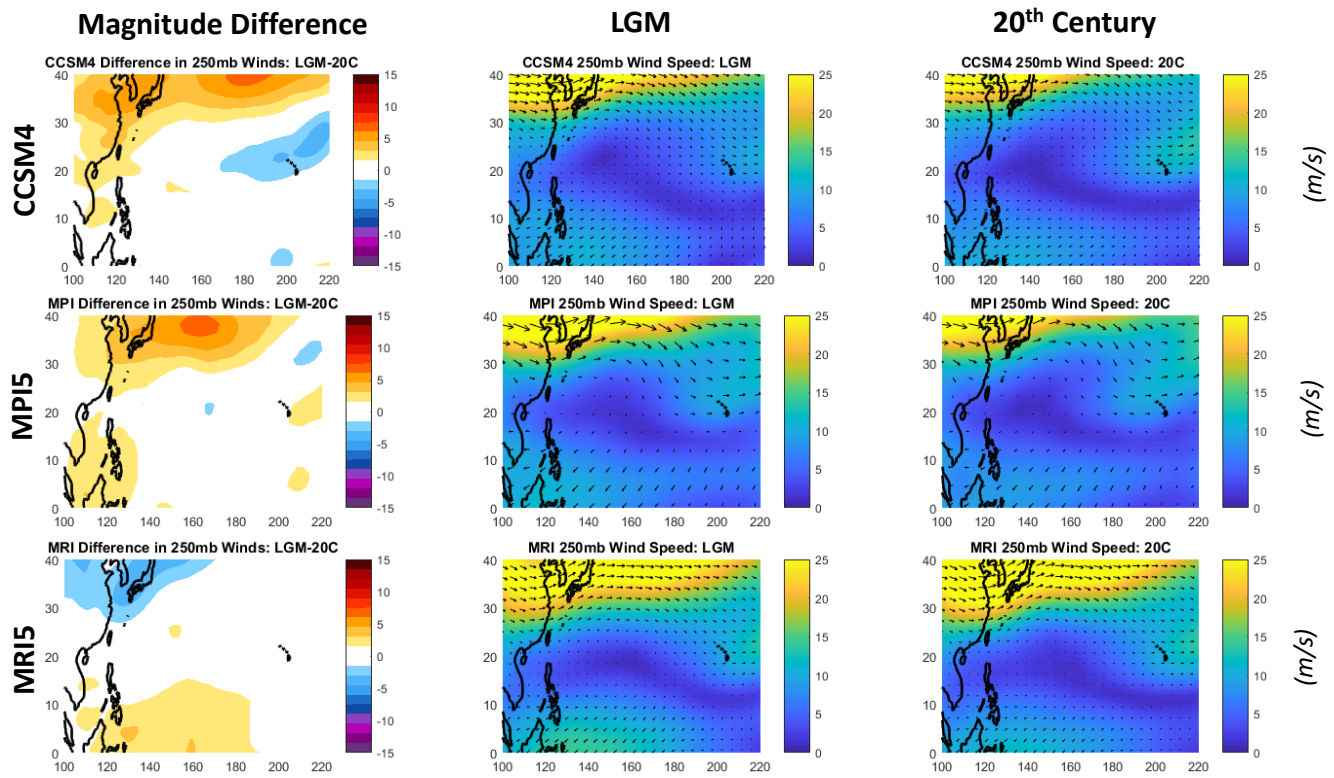

Figure 19- Simulation and climate state comparision of storm-season avearge 250mb wind speed and direction in the Western North Pacific Basin. Shaded contours are of the absolute magintude of average wind speed, and plotted vectors show the average 250mb wind direction. Units are m/s.

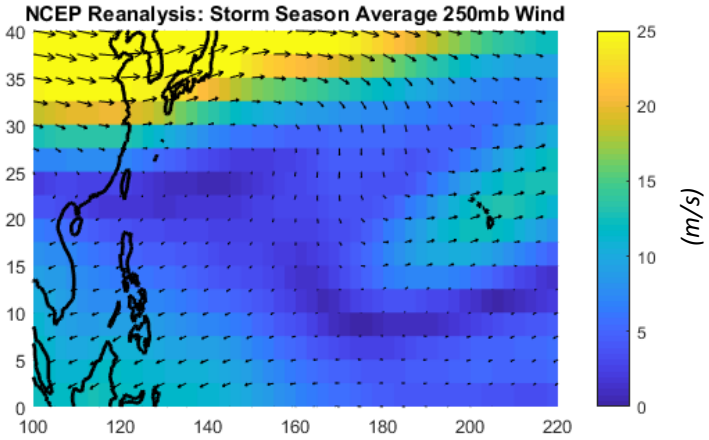

Figure 20- Climatological storm-season average 250mb wind speed and direction from 1948-2017. Units are m/s. NCEP Reanalysis data provided by the NOAA/OAR/ESRL PSD, Boulder, Colorado, USA, from their Web site at https://www.esrl.noaa.gov/psd/. Further information can be found in Kalnay et. al. (1996).

In all three models, decreased LGM TC favorability appears somewhat tied to the strengthening of the Northeastern Trade winds at 250mb between 0° and 15°N latitude. The extent of these strengthened trade winds varies by circulation; the MRI simulation extends this region into the majority of formation regions for the Western North Pacific, the CCSM4 shows relatively minimal changes in the trade winds, and the MPI simulation falls somewhere in between these two extremes. Meanwhile, the CCSM4 and MPI show some areas of decreased LGM upper-level winds in the eastern part of the basin and extending into the Central Pacific. This may have contributed to reduced LGM wind shear shown for these regions in Figure 18. Areas with minimal changes in 250mb wind magnitude- such as in the Central and Southern portions of the North Pacific- likely saw 850mb winds patterns having the primary influence on wind shear. Future analysis of 850mb wind patterns and associated temperature gradients is necessary to better understand the underlying changes influencing wind shear in the Western North Pacific.

Interestingly, while both the CCSM4 and MPI simulations depict a stronger mid-latitude jet stream during the LGM as compared to the 20th Century, the MRI simulation depicts a weakened LGM jet stream. This could result from variations in each model's depiction of temperature gradients in this region. Future work is needed to better understand these temperature deviations and their underlying sources. Whatever their cause, variations in the mid-latitude jet stream and Central Pacific wind patterns likely have less of an impact on downscaled TCs than other regions. This is primarily due to the relatively fewer TCs that form or move into these areas. However, investigating how these wind patterns modulate latitudinal TC extent could prove insightful in future studies.

All three models depict upper-level wind flow in the deep tropics relatively accurately when compared to the observed climatology (Figure 20). Some deviations become apparent north of 20°N, with MRI again being the outlier of the two models. The MRI has a much stronger mid-latitude jet in the plotted region (0 to 40°N) and extends much further east than observed climatology. The other two simulations (CCSM4 and MPI) pair with climatology much more closely.

With anomalous solutions to upper-level wind patterns in both the Western North Pacific and the Northern Atlantic, the MRI's accuracy in representing atmospheric flow in the Northern Hemisphere seems questionable. However, with only a larger pool of simulations to compare to and a lack of detailed analysis of other environmental characteristics and atmospheric levels, it is hard to quantify how impactful model inaccuracies are on downscaled TCs. We also lack the information to know how these errors might extrapolate to other paleoclimates or projects. Nevertheless, we can conclude that deviations in the MRI's simulations of atmospheric circulations likely played a significant impact in modifying the behavior of downscaled TCs.

Impacts of the El Niño-Southern Oscillation

Previous studies have linked phases of the El Niño-Southern Oscillation (ENSO) to global TC climatology. Gray (1984) was the first to link the ENSO warm phase- known as El Niño- to decreased TC activity in the Atlantic. This is thought to result from increased wind shear in the Atlantic basin during the ENSO warm phase, which is detrimental to TC development (Gray 1968; Gray 1984). Similarly, the ENSO cool phase- La Niña- reduces wind shear in the Atlantic Basin, increasing the favorability of TCs. In the Western North Pacific, TC activity is also modulated by ENSO phase. It has been shown that the number of TCs in the

Western Pacific basin decreases during El Niño years- specifically landfalling TCs and storm in the western part of this region (Chan 1984; Wu et. al. 2003).

Analyzing a period of time with an unequal number or magnitude of opposing ENSO phases could modulate overall TC characteristics, especially when focused on specific basins. Thus, we studied ENSO in our utilized models to identify its impact on overall results. To define ENSO phase, we analyzed SST anomalies within the Niño 3.4 region in the manner prescribed by Trenberth (1997). An ENSO phase occurs when the 5-month running mean exceeds $\pm \mathbf{0.4°C}$ of the monthly mean for 6 consecutive months. This was done for each model, with the results shown in Table 6.

Table 6

ENSO events defined by 6+ consecutive monthly SST anomalies of +-0.4°C: Niño 3.4 Region						
Models	**CCSM4**		**MPI5**		**MRI5**	
	LGM	20C	LGM	20C	LGM	20C
El Niño Phases	8	3	5	5	4	3
La Niña Phases	5	5	4	4	3	2

Both the MPI and MRI models have a similar number of positive and negative ENSO events within each climate state, with only slight variability. The CCSM4 model, however, has a consistent number of La Niña events for each climate state, but has significantly more El Niño events (8) in the LGM than in the 20th Century (3). This leads to asymmetry in ENSO events within each CCSM4 climate state, and with it the potential for modified TC activity. This pattern is further evident in the comparative timeseries of Niño 3.4 SST anomaly shown in Figure 21.

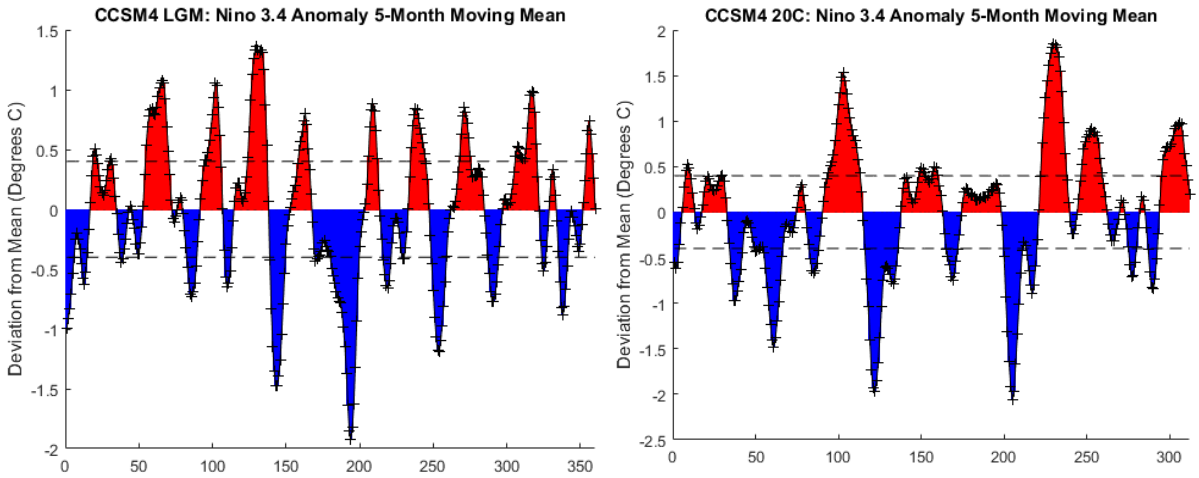

Figure 21- A comparison of 5-month moving mean of SST anomaly (from the monthly average) within the Niño 3.4 region throughout the analyzed temporal period. Dashed black lines indicate the thresholds for the positive and negative ENSO phases, and the area under the curve is filled in based on the direction of SST anomaly from the mean values. Red indicates positive SST anomalies, and blue indicates negative SST anomalies.

The CCSM4 LGM climate state appears to have a much higher frequency of ENSO oscillation with more positive events meeting the threshold of El Niño. We must be wary of the rigid, categorical cutoffs used in this calculation of ENSO phases, as there is no precise universal definition of ENSO (Trenberth 1997). Nevertheless, this apparent increase in El Niño events during the LGM could have modulated TC behavior, especially in the Atlantic and Western Pacific regions where El Niño has been shown to reduce TC activity. Furthermore, while MRI and MPI both had fewer asymmetries in number of events, this does not consider the precise strength or duration of each phase. Future analysis is needed to determine the influence of any asymmetries in ENSO strength and duration. Understanding how ENSO phase directly impacts environmental conditions in each simulation could also prove insightful. For now, we acknowledge that ENSO very well could have played a role in the modification of downscaled TCs through their residual environment, but that more analysis is needed.

CHAPTER IV

CONCLUSION

Summary of Results

In this analysis, we evaluated the variability in TC genesis factors between three models' simulations of the LGM and 20th Century to determine how this affected the properties of downscaled TCs. Characteristics were studied globally and regionally within the Western North Pacific and North Atlantic basins. We focused on Power Dissipation Index (PDI) of downscaled TCs as our integrated measure of how TC strength changed between climate states and differed between models. This behavior was compare to modifications in environmental parameters including 850mb to 250mb wind shear, potential intensity (PI), relative sea-surface temperatures (RSST), and upper-level wind speed. The two components thought to contribute most to TC favorability- potential intensity and vertical wind shear- were weighted in a combined-metric developed in Bruyère et. al. (2012) called Cyclone Genesis Index (CGI). Connections were made to large-scale shifts in atmospheric and oceanic circulations. Changes in wind shear in the Northern Atlantic were tied to the weakening (or in the case of the MRI, strengthening) of the sub-tropical jet over Africa visible at 250mb. In the Western North Pacific, shifts in the 250mb trade winds explained some modulations of wind shear at low latitudes and towards the continental boundary. The statistical significance of storm-season averages for most analyzed parameters were also evaluated for defined basins and at each simulated grid-point.

As one measure of TC events, we indirectly computed the average annual frequency of TCs in each simulation and climate state. While this method did not allow direct comparisons between simulations (see results section for more details), intra-model changes were considered

reliable for comparison. Two of our simulations- the CCSM4 and the MPI- showed a general increase in the annual frequency with warming from the cooler LGM climate to the warmer 20th Century. The MRI simulation, however, showed a slight reduction in this frequency with warming. This inter-model variability is analogous to the current uncertainty in the relationship between TC frequency and warming climate, although most general-circulation models show a decline in directly simulated events with projections of warming (Sobel 2016). Statistical downscaling, such as what was used in this analysis, has often shown an increase in TC events with warming (e.g. Emanuel et. al. 2008, Emanuel 2013).

In all three models, warming from the LGM to the 20th Century resulted in an increase in the proportion of downscaled TCs reaching high intensities (Category 4 and 5). The majority of TCs in each simulation did not exceed Tropical Storm or Category 1 strength. While the specific cause for model variation in low-intensity TCs response was not determined in this analysis, it is likely inconsequential. Overall, changes in intensity distribution for all three models aligned with theoretical and simulated TC response in future climate projections (e.g. Sobel 2016, Knutson et. al. 2015, Bender et. al. 2010).

Regionally, downscaled TC PDI and environmental CGI often increased in analyzed ocean basins. An increase in TC PDI and CGI favorability was seen from the LGM to the 20th Century for all three models within the primary (western) region of the Western North Pacific Basin. The two major environmental factors associated with these changes were RSST- which generally increased from the LGM to the 20th Century along the continental boundary- and wind shear -which generally experienced wide-scale decreases from the LGM to 20th Century (with some variation in CCSM4). It should be noted that RSST, by definition, must average out to zero in the tropics (30°S to 30°N), making its changes highly regionalized. Similarly, two simulations

in the Atlantic basin- CCSM4 and MPI- showed an increase in TC PDI in the warmer 20th Century climate. This suggests increased distributions of TC intensity within these two regions- both of which are major TC formation regions- largely aligning with the projected response to future warming (Sobel 2016).

Deviations from this trend were also seen in specific models and regions. In the Northern Atlantic basin, the MPI model depicted generally lower TC PDI and CGI favorability as the climate warmed. This was found to be primarily due to an increase in the strength of the subtropical jet during the 20th Century. This highlights the impact vertical wind shear can have in decreasing the environmental favorability of TCs, as has been shown in previous studies (Gray 1968; Vecci and Soden 2007; Gu et. al. 2015; Sobel 2016). This region also had decreasing RSSTs with warming climate, which corresponded to a similar decrease in PI with warming. However, the significance of this result is questionable primarily due to significant deviations in the MPI model depiction of the 20th Century from modern climatology. These deviations are predominantly seen in the MRI's simulation of upper-level wind patterns within the Western North Pacific and North Atlantic. Nevertheless, this result underlines the important role circulation patterns play in governing TC response to changing climate.

While typically changes in PDI were shown to correspond to changes in CGI, PI, and shear, this was not always the case. A pronounced exception occurred in the MPI simulation within the North Pacific Basin, where CGI direction did not obviously correspond with changes in PDI in the secondary (eastern) region. This suggests that the use of other combined metrics for TC favorability should also be compared to that of CGI and individual environmental parameters. GPI is discussed earlier as an empirically-derived function first developed by Emanuel and Nolan (2004) estimating the combined influence of various environmental

conditions on TC development, and ventilation is theorized by Tang and Emanuel (2010) as a fundamental measure of how environmental influencers such as vertical wind shear decrease thermodynamic efficiency in TCs. Comparing these parameters with our results could give a better indication of how robust each metric is for a given model or region.

Future Work

There exist several avenues on which to expand this analysis. For one, we primarily analyzed trends in annual frequency, intensity distributions, and PDI. However, there are additional TC characteristics that can be studied, including TC track density, TC genesis density, TC size, and the frequency of landfalling storms. Learning how these additional properties of the TC climatology change in relation to PDI and the residual environment could prove insightful for further quantifying the impact of changing climate on TCs. Improvements could also be made in utilizing combined metrics. In this analysis, we used CGI to combine the impacts of PI and vertical wind shear when studying the residual environment of downscaled TCs. CGI correlated well to downscaled TC behavior in most cases, but it also failed to explain changes in one region in the Western North Pacific. It is also unknown how well CGI will work across a larger variety of models and ocean basins. Thus, future analysis should compare several additional combined metrics to CGI- such as ventilation and GPI- to see which metric remains the most robust in different regions and models.

Additional work is needed to better quantify the atmospheric patterns that lead to changes in TC favorability. This include further analyzing 850mb level winds to better determine their influence on wind shear- especially in regions such as the Western North Pacific where the 850mb level likely contributed to calculated wind shear as much or more than the 250mb level.

Identifying temperature gradients and their relation to model parameterization would assist in determining the root cause of regional and inter-model variation in wind patterns.

As discussed in the methods and results chapters, our spatial investigation focused on two ocean basins- the Northern Atlantic and the Western North Pacific. However, downscaled TCs were generated across the globe. As our method can be applied in all major TC basins, we anticipate important information could obtained from studying downscaled TC and environment trends within the Indian Ocean and Southern Hemispheric basins.

Finally, further work is needed to better quantify the effect of specific oceanic circulations and internal climate oscillations on TCs synthesized from these simulations. This especially includes the impact of ENSO. Our results indicated that the CCSM4 model had an asymmetry in ENSO phase in both climate states. This could have impacted the observed patterns in downscaled TCs, as could have variations in ENSO strength within other simulations. Further quantifying the impact ENSO events have on environmental conditions and downscaled TCs would assist in isolating the impact of ENSO from that of the overall warming climate. Additional work is also needed to determine the root cause of changes in RSST and PI in relation to oceanic and atmospheric heat transport. Further identifying how these underlying circulations modify TCs would improve our fundamental understanding on how TCs may respond to similar changes in the future.

REFERENCES

Anthes, R. A., 1982: *Tropical Cyclones: Their Evolution, Structure and Effects*, American Meteorological Society, 208 pp.

Bender, M. A., T. R. Knutson, R. E. Tuleya, J. J. Sirutis, G. A. Vecchi, S. T. Garner, and I. M. Held, 2010: Modeled Impact of Anthropogenic Warming on the Frequency of Intense Atlantic Hurricanes, *Science*, **327**, 454-458. doi:10.1126/science.1180568

Bister, M. and K. A. Emanuel, 2002: Low frequency variability of tropical cyclone potential intensity, 1, Interannual to interdecadal variability. *J. Geophys. Res.*, **107**, 4801, doi: 10.1029/2001JD000776

Braconnot, P., B. Otto-Bliesner, S. Harrison, S. Joussaume, J. -Y. Peterchmitt, A. Abe-Ouchi, M. Crucifix, E. Driesschaert, Th. Fichefet, and C. D. Hewitt, 2007: Results of PMIP2 coupled simulations of the Mid-Holocene and Last Glacial Maximum- Part 1: experiments and large- scale features. *Clim. Past*, **3**, 261-277.

Braconnot, P., S. P. Harrison, M. Kageyama, P. J. Bartlein, V. Masson-Delmotte, A. Abe-Ouchi, B. Otto-Bliesner, and Yan Zhao, 2012: Evaluation of climate models using palaeoclimatic data. *Nat. Clim. Change*, **2**, 417–424, doi:10.1038/NCLIMATE1456

Brady, E. C., B. L. Otto-Bliesner, J. E. Kay, and N. Rosenbloom, 2013: Sensitivity to Glacial Forcing in the CCSM4. *J. Climate*, **26**, 1901-1925, doi:10.1175/JCLI-D-11-00416.1

Broccoli, A. J., 2000: Tropical Cooling at the Last Glacial Maximum: An Atmosphere-Mixed Layer Ocean Model Simulation. *J. Climate*, **13**, 951-976.

Bruyère, C. L., G. J. Holland, and E. Towler, 2012: Investigating the Use of a Genesis Potential Index for Tropical Cyclones in the North Atlantic Basin. *J. Climate*, **25**, 8611-8626, doi:10.1175/JCLI-D-11-00619.1

Bryan, G. H., and R. Rotunno, 2009: Evaluation of an analytical model for the maximum intensity of tropical cyclones. *J. Atmos. Sci.*, **66**, 3042–3060, doi:10.1175/2009JAS3038.1.

Chan, J. C. L., 1984: Tropical Cyclone Activity in the Northwest Pacific in Relation to the El Niño/Southern Oscillation Phenomenon. *Mon. Weather Rev.,* **113**, 599-606, doi:https://doi.org/10.1175/1520-0493(1985)113<0599:TCAITN>2.0.CO;2

Denommee, K. C., S. J. Bentley, and A. W. Droxler, 2014: Climatic controls on hurricane patterns: a 1200-y near-annual record from Lighthouse Reef, Belize. *Scientific Reports*, **4**, 3876, doi:10.1038/srep03876

Donnelly, J. P., S. Roll, M. Wengren, J. Butler, R. Lederer, and T. Webb III, 2001: Sedimentary evidence of intense hurricane strikes from New Jersey. *Geology*, **29**, 615-618, doi:10.1130/0091-7613(2001)029<0615:SEOIHS>2.0.CO;2

Emanuel, K. A., 1986: An Air-Sea Interaction Theory for Tropical Cyclones. Part I: Steady-State Maintenance. *J. Atmos. Sci,* **46**, 585-604.

Emanuel, K. A., 1995: Sensitivity of tropical cyclones to surface exchange coefficients and a revised steady-state model incorporating eye dynamics. *J. Atmos. Sci.*, **52**, 3969–3976.

Emanuel, K. A., 2003: Tropical Cyclones. *Annu. Rev. Earth Planet. Sci.,* **31**, 75-104, doi:10.1146/annurev.earth.31.100901.141259

Emanuel, K. A., C. DesAutels, C. Holloway, and R. Korty, 2004: Environmental control of tropical cyclone intensity. *J. Atmos. Sci.,* **61**, 843-858.

Emanuel, K. A., 2005: Increasing destructiveness of tropical cyclones over the past 30 years. *Nature,* **436**, 686-688. doi:10.1038/nature03906.

Emanuel, K. A., 2006: Climate and tropical cyclone activity: A new model downscaling approach. *J. Climate,* **19**, 4797-4802.

Emanuel, K. A., 2013: Downscaling CMIP5 climate models shows increased tropical cyclone activity over the 21st century. *Proc. Natl. Acad. Sci. U.S.A,* **110**, 12219-12224, doi:10.1073/pnas.1301293110

Emanuel, K. A., 2015: Effect of Upper-Ocean Evolution on Projected Trends in Tropical Cyclone Activity, *J. Climate,* **28**, 8165-8170. doi:10.1175/JCLI-D-15-0401.1

Emanuel, K. A., and D. S. Nolan, 2004: Tropical cyclone activity and the global climate system. Preprints, *26th Conf. on Hurricanes and Tropical Meteorology*, Miami, FL, Amer. Meteor. Soc., 10A.2.

Emanuel, K. A., R. Sundararajan, and J. Williams, 2008: Hurricanes and Global Warming, Results from Downscaling IPCC AR4 Simulations. *BAMS*, **89**, 347-367, doi:10.1175/BAMS-89-3-347

Federov, A. V., C. Brierly, and K. A. Emanuel, 2010: Tropical cyclones and permanent El Niño in the early Pliocene epoch. *Nature*, **463**, 1066-1070, doi:10.1038/nature08831

Gray, W., 1968: Global View of the Origin of Tropical Disturbance and Storms. *Mon. Weather Rev.*, **96** (10), 669-700, doi:10.1175/1520-0493(1968)096<0669:GVOTOO>2.0.CO;2

Gray, W., 1984: Atlantic Seasonal Hurricane Frequency. Part I: El Niño and 30 mb Quasi-Biennial Oscillation Influences. *Mon. Weather Rev.*, **112**, 1649-1668, doi:10.1175/1520-0493(1984)112<1649:ASHFPI>2.0.CO;2.

Gu. JF., Tan ZM., and X. Qiu, 2015: Effects of Vertical Wind Shear on Inner-Core Thermodynamics of an Idealized Simulated Tropical Cyclone. *J. Atmospheric Sci.*, **72**, 511-530. doi:10.1175/JAS-D-14-0050.1

Holland, G. J., 1997: The Maximum Potential Intensity of Tropical Cyclones. *J. Atmospheric Sci.*, **54**, 2519-2541, doi:10.1175/1520-0469(1997)054<2519:TMPIOT>2.0.CO;2

Kalnay et al., 1996: The NCEP/NCAR 40-year reanalysis project. *Bull. Amer. Meteor. Soc.*, **77**, 437-470.

Koh, J. H. and C. M. Brierly, 2015: Tropical cyclone genesis potential across palaeoclimates. *Clim. Past*, **11**, 1433-1451, doi:10.5194/cp-11-1433-2015

Korty, R. L., S. J. Camargo, and J. Galewsky, 2012: Tropical Cyclone Genesis Factors in Simulations of the Last Glacial Maximum. *J. Climate*, **25**, 4348-4365, doi:10.1175/JCLI-D-11-00517.1

Korty, R. L., K. A. Emanuel, M. Huber, and R. A. Zamora, 2017: Tropical Cyclones Downscaled from Simulations with Very High Carbon Dioxide Levels. *J. Climate,* **30**, 649-667, doi:10.1175/JCLI-D-16-0256.1

Knutson, T. R., J. J. Sirutis, and M. Zhao, 2015: Global Projections of Intense Tropical Cyclone Activity for the Late Twenty-First Century from Dynamical Downscaling of CMIP5/RCP4.5 Scenarios, *J. Climate*, **28**, 7203-7224, doi:10.1175/JCLI-D-15-0129.1

Liu, K. B. and M. L. Fearn, 1993: Lake-Sediment Record of Late Holocene Hurricane Activities from Coastal Alabama. *Geology,* **21,** 793-796, doi:10.1130/0091-7613(1993)021<0793:LSROLH>2.3.CO;2

Murakami, H., R. Mizuta, and E. Shindo, 2012: Future changes in tropical cyclone activity projected by multi-physics and multi-SST ensemble experiments using the 60-km-mesh MRI-AGCM, *Clim. Dyn*, **39**, 2569-2584. doi:10.1007/s00382-011-1223-x

Otto-Bliesner, B. L., and B. C. Esther, 2006: Last Glacial Maximum and Holocene Climate in CCSM4. *J. Climate,* **19**, 2526-2544.

Saffir, H. S., 1973: Hurricane Wind and Storm Surge. *The Military Engineer*, **423**, 4-5.

Schmidt, G. A., J. H. Jungclaus, C. M. Atmmann, E. Bard, P. Braconnot, T. J. Crowley, G. Delaygue, F. Joos, N. A. Krivova, R. Muscheler, B. L. Otto-Bliesner, J. Pongratz, D. T. Shindell, S. K. Solanki, F. Steinhilber, and L. E. A. Vieira, 2011: Climate forcing reconstructions for use in PMIP simulations of the last millennium (v1.0). *Geosci. Model Dev.*, **4,** 33-45, doi:10.5194/gmd-4-33-2011

Simpson, R. H., 1974: The Hurricane Disaster Potential Scale, *Weatherwise*, **27**, 169-186.

Sobel, A. H., S. J. Camargo, T. M. Hall, C. Lee, M. K. Tippett, and A. A. Wing, 2016: Human influence on tropical cyclone intensity. *Science*, **353**, 242-246, doi:10.1126/science.aaf6574

Southern, R. L., 1979: The global socio-economic impact of tropical cyclones. *Aust. Meteorol. Mag.*, **27**, 175-195.

Ramsay, H. A. and A. H. Sobel, 2010: Effects of Relative and Absolute Sea Surface Temperature on Tropical Cyclone Potential Intensity Using a Single-Column Model. *J. Climate*, **24**, 183-193.

Tang, B., and K. A. Emanuel, 2010: Midlevel Ventilation's Constraint on Tropical Cyclone Intensity. *J. Atmos. Sci.*, **67**, 1817-1830, doi:10.1175/2010JAS3318.1

Taylor, K. E., R. J. Stouffer, G. A. Meehl, 2009: A Summary of the CMIP5 Experiment Design. [https://pcmdi.llnl.gov/mips/cmip5/experiment_design.html]

Taylor, K. E., R. J. Stouffer, G. A. Meehl, 2012: An Overview of CMIP5 and the experiment design. *Bull. Amer. Meteor. Soc.*, **93**, 485-498, doi:10.1175/BAMS-D-11-00094.1

Toomey, M. R., W. B. Curry, J. P. Donnelly, and P. J. van Hengstum, 2013: Reconstructing 7000 years of North Atlantic hurricane variability using deep-sea sediment cores from the western Great Bahama Bank. *Paleoceanography*, **28**, 31-41, doi:10.1002/palo.20012

Toomey, M. R., R. L. Korty, J. P. Donnelly, P. J. van Hengstum, and W. B. Curry, 2017: Increased hurricane frequency near Florida during Younger Dryas Atlantic Meridional Overturning Circulation slowdown. *Geology*, **45**, 1047-1050, doi:10.1130/G39270.1

Trenberth, K. E., 1997: The Definition of El Niño. *Bull. Amer. Meteor. Soc.*, **78**, 2771-2777.

Wang, S., S.J. Camargo, A.H. Sobel and L.M. Polvani, 2014: Impact of the tropopause temperature on the intensity of tropical cyclones - an idealized study using a mesoscale model. *J. Atmos. Sci.*, **71**, 4333-4348, doi:10.1175/JAS-D-14-0029.1.

Wu, M. C., W. L. Chang, and W. M. Leung, 2003: Impacts of El Niño-Southern Oscillation Events on Tropical Cyclone Landfalling Activity in the Western North Pacific. *J. Climate*, **17,** 1419-1428

Vecchi, G. A., and B. J. Soden, 2007: Effect of remote sea surface temperature change on tropical cyclone potential intensity. *Nature*, **450**, 1066–1070.

Yu. J, Y. Wang, K. Hamilton, 2010: Response of Tropical Cyclone Potential Intensity to a Global Warming Scenario in the IPCC AR4 CGCMs. *J. Climate*, **23**, 1354-1373, doi:10.1175/2009JCLI2843.1